

Interpreting GNN-based IDS Detections Using Provenance Graph Structural Features

Kunal Mukherjee, Joshua Wiedemeier, Tianhao Wang, Muhyun Kim, Feng Chen,
Murat Kantacioglu, and Kangkook Jee

Department of Computer Science, The University of Texas at Dallas

Abstract— Advanced cyber threats (e.g., Fileless Malware and Advanced Persistent Threat (APT)) have driven the adoption of *provenance-based* security solutions. These solutions employ Machine Learning (ML) models for behavioral modeling and critical security tasks such as malware and anomaly detection. However, the opacity of ML-based security models limits their broader adoption, as the lack of transparency in their decision-making processes restricts explainability and verifiability. We tailored our solution towards Graph Neural Network (GNN)-based security solutions since recent studies employ GNNs to comprehensively digest system provenance graphs for security critical tasks.

To enhance the *explainability* of GNN-based security models, we introduce PROVEXPLAINER, a framework offering *instance-level security-aware* explanations using a interpretable surrogate model. PROVEXPLAINER’s interpretable feature space consist of *discriminant subgraph patterns* and *graph structural features* which can be directly mapped to the system provenance problem space, making the explanations human understandable. Considering both the subgraph patterns and graph structural features, gives PROVEXPLAINER the unique advantages of providing explanations that are sensitive to both local as well as global changes.

By considering prominent GNN architectures (e.g., GAT and GraphSAGE) for program classification and anomaly detection tasks, we show how PROVEXPLAINER synergizes with current state-of-the-art (SOTA) GNN explainers to deliver domain and instance specific explanations. We measure the explanation quality using fidelity⁺ /fidelity⁻ metric as used by traditional GNN explanation literature, and we incorporate the precision/recall metric where we consider the accuracy of the explanation against the ground-truth. On malware and APT datasets, PROVEXPLAINER achieves up to 29% / 27% / 25% higher fidelity⁺ , precision and recall, and 12% lower fidelity⁻ respectively, compared to SOTA GNN explainers.

1. Introduction

Given the significant threat posed by advanced and sophisticated adversaries [1]–[4] (i.e., malware writers and APT actors), security is paramount in today’s highly digitized society. Recent advances in system monitoring have

generated a variety of fine-grained telemetry for advanced security analysis. To leverage this telemetry to counter security threats, various learning-based security tools have been proposed and deployed [5]–[21]. System provenance captures causally dependent system events on an end host, represented as a provenance graph. Provenance graphs are heterogeneous, comprising various node types (e.g., process, file, and socket) and edge types (e.g., read, write, and send), each with textual and numerical attributes, effectively representing dynamic runtime behaviors. Hence, provenance graphs provide irreplaceable security defense for countering sophisticated and stealthy APT-like attack campaigns. Particularly, Endpoint Detection and Response (EDR) solutions [22]–[24], built on fine-grained system provenance data, have become a mainstream security defense for enterprise networks [25], [26].

The increasing use of provenance graphs has spurred interest in leveraging Graph Neural Networks (GNNs) for security applications. Recent advancements in GNNs enable the direct learning of relational dependencies and topological structures from graphs. GNNs utilize a permutation-invariant message-passing mechanism to aggregate information from node neighborhoods, expanding the information propagated through each neighborhood with every iteration. This allows GNNs to learn from complex graph structures automatically, which has proven beneficial for provenance-based security solutions [19]–[21], [27]. However, while GNN-based security models are highly effective, their opaque nature significantly limits their advantages, particularly due to the lack of clear, verifiable explanations for their predictions. These models fail to provide *ground-truth relevant* explanations, which are essential for building trust among security practitioners. In this context, ground-truth relevant explanations refer to explanations aligned with specific system actions that represent techniques, procedures, and system artifacts that are familiar to security professionals and can be validated by existing ground-truth intelligence.

While studies [28]–[30] have explored domain-agnostic explanations for GNN decisions, they lack validation in the security domain, where contextualizing explanations with program behaviors is critical for trust in the underlying model. Recent research [31]–[33] has emphasized verifiable explanations for neural networks in binary analysis and

vulnerability discovery, yet *our study is the first to validate explanations within the system provenance domain*. Traditional explainable Machine Learning (ML) techniques [34], [35] have focused on explanations based on the model’s input or internal parameters; however, such explanations may be inadequate or unintelligible for end-users in cybersecurity, where a single error can have catastrophic outcomes. Explanations have different meaning for model developers and end-user, since end-users cannot make sense of explanations in terms of model weights or gradients, but can make sense if explanations are in terms of edges or subgraphs. In security domain, models must explain their decision-making processes [36] that are verifiable using the ground-truth.

In this paper, we introduce a novel approach to enhance the explainability of GNN models based on system provenance data by integrating an interpretable surrogate model, specifically Decision Trees (DT), with security-aware *discriminant subgraph patterns* and *graph structural features*. We efficiently mined subgraph patterns [37] using a graph evolution miner (GERM [37]) to identify discriminative subgraph patterns between malicious and benign datasets. Additionally, we extracted structural graph features, such as degree centrality, betweenness centrality, closeness centrality, eigenvector centrality, clustering coefficient, and triangle clustering. These structural features capture long-term dependencies within the system, while the subgraph patterns represent local dependencies. Together, they provide explanations for both short-term and long-term dependencies in the graph. Our analysis revealed that these subgraph patterns correspond to well-known malicious activities, such as drive-by-downloads (e.g., dropper malware)[38], [39], malware staging and propagation[40], system probing [41], and malware replication using templates [42]. By incorporating these features alongside graph structural measures, our model facilitates interpretability for security experts [43] by closely aligning with security-relevant system behaviors.

While our research takes full advantage of an extensive dataset that we collected from real systems, we specifically focus on the structural features of system provenance graphs, without considering the text or numerical node and edge attributes. We restrict the scope of our attribute view for the following reasons: first, the core merit of provenance based Intrusion Detection System (IDS) lies in the ability to retain features drawn from causal dependencies captured in graph structural relations; these structural features are significantly more difficult for adversaries to manipulate than textual attributes (e.g., filenames). Secondly, if we cannot adequately explain GNN decisions based solely on structural features, it becomes even more challenging to interpret decisions when GNNs incorporate both structural and attribute-based complexities.

Our research effort decouples the feature engineering and decision-making processes of GNN models, focusing on feature engineering to support *human interpretability* rather than solely improving decision accuracy. The core insight behind our study is that general-purpose explanation techniques lack security-specific considerations but can be enhanced with tailored structural features to address this

gap. We emphasize that PROVEXPLAINER is an explanation framework, not an attack detection technique. Unlike GNNs, surrogate Decision Trees (DTs) sacrifice generalizability, expressiveness, and automatic feature extraction to gain interpretability, making them unsuitable for direct attack detection. PROVEXPLAINER is a GNN-structure-agnostic framework capable of incorporating an arbitrary number of subgraph patterns and structural graph features, and it is designed for easy extensibility with additional security-aware graph features.

We measured the effectiveness of PROVEXPLAINER using fidelity⁺ and fidelity⁻ similar to previous GNN explainability research [30]. We also incorporated two additional measure known as precision and recall that captures the accuracy of the explanation provided compared against the ground-truth. While PROVEXPLAINER independently surpasses current State-Of-The-Art (SOTA) GNN explainers in the majority of our security-oriented evaluation tasks, as we show in our experimental evaluation, it can also be seamlessly integrated with other SOTA GNN explainers to develop even more effective explanations. Notably, our research does not attempt to completely replace existing GNN model explanation approaches. While stable and accountable, PROVEXPLAINER’s coverage is inherently limited by the capacity of our surrogate DT architecture. We intend PROVEXPLAINER to be complementary to a large body of existing literature on GNN model explanations with specific emphasis on security domain constraints and their interpretability.

To demonstrate the advantages of PROVEXPLAINER in the system provenance domain, we compared PROVEXPLAINER against SOTA GNN explainers such as GNNExplainer [28], PGExplainer [29], and SubgraphX [30] across well-balanced security domain tasks, including malware detection, and APT detection. These SOTA GNN explainers provide the best performance according to other security studies [32], [44]. The GNN models in our evaluation are trained with an extensive dataset collected using our in-house deployment which monitored system events on an average of 20 mixed Windows and Linux hosts over 13 months. In addition, in our evaluation, we used the DARPA [45] Transparent Computing dataset, the APT dataset from [46], and malware lists from [47].

To our knowledge, our research is the first to leverage security-aware discriminant subgraph pattern and graph structural features specifically tailored for human interpretation. Broadly, we summarize the contributions of PROVEXPLAINER as follows:

- PROVEXPLAINER examines discriminant subgraph patterns and graph structural features to provide GNN detection explanation.
- Our security-aware features enabled surrogate DTs to achieve 95% agreement with the GNN model on malware and APT attack detection.
- PROVEXPLAINER improves fidelity⁺ by 29%, precision by 27%, recall by 25% and decreased fidelity⁻ by 12% compared to SOTA GNN explainers: GNNExplainer [28], PGExplainer [29], and SubgraphX [30].

TABLE 1: Node and edge types for in-house system provenance with associated attributes.

	Types	Attributes
Nodes (resources)	process file socket (IP)	signature, executable name, pid owner (uid, gid), name, inode dstip, srcip, dstport, srcport, type
Edges (events)	process → process process → file process → IP address	command args, starttime read, write, amount send, recv, amount

- We curated an extensive dataset using in-house data collection, APT datasets from different sources (*i.e.*, DARPA [45] and past literature [46]) and collected real-world malware samples from [47] to confirm the generalizability of PROVEXPLAINER.

To benefit the community and facilitate future research, we are committed to publish our dataset and code.

2. Background and Related Work

We introduce system provenance and ML security applications using it. We discuss the efforts made to explain GNN models and their challenges. We discuss the verification of explanations in the system provenance domain.

2.1. System Provenance and Data Collection

System provenance analysis [48], [49] leverages data collection agents on end-hosts to collect interaction events among key system resources: processes, files, and network sockets. This work relies on in-house data from 21 hosts in a university environment, the DARPA Transparent Computing dataset [45], and datasets from previous study [46]. Our in-house data collection accumulates 13 GB to 92 GB daily, tracking around 875 unique programs, 7,025K processes, 4,824K network connections, and 111,583K file operations.

Our system provenance data schema, detailed in Table 1, is similar to DARPA’s Common Data Model (CDM) [45] schema, but we omit memory objects, registry events, and thread distinctions within a process. These choices were made to balance real-world overhead constraints of load balancing and storage. We also established a malicious testbed to generate malware execution traces. To ensure the freshness and realism of our malware samples, we utilize Cyber Threat Intelligence (CTI) feeds [50], the VirusTotal database [51], and penetration testing tactics, techniques, and procedures (TTPs) [52]–[54]. We refer to DARPA TC dataset [45] and previous literature of [46] for APTs.

2.2. Provenance-based ML Security Solutions

Recent advancements in system event collection have revitalized host-based IDSs. Although initially proposed in the late ’90s [55], host-based IDSs have proved effective against advanced attacks such as APTs and Fileless Malware. Various studies [15], [18]–[21], [56], [57] demonstrate the efficacy of provenance-based ML techniques in identifying

behavioral deviations. However, the high detection performance is offset by a lack of trustworthy explanations and high false positive rates, impacting operational confidence and resource allocation. Detection tasks are prone to errors and are difficult to verify without full knowledge of typical behaviors. Our work focuses on enhancing the transparency and explainability of provenance-based ML security. We concentrate on a balanced set of security tasks of malware and APT detection. In this paper, we consider graph-level tasks; providing explanations for node and edge level tasks is a promising direction for future work that aligns with upcoming security detection system trends.

GNNs for System Provenance. Our research employs an industry-standard GNN framework (*i.e.*, Deep Graph Learning (DGL)) [58] to model and explain system provenance graphs. Leveraging DGL’s mature development ecosystem PROVEXPLAINER aligns with current analytical techniques and streamlined integration into real-world applications. Despite the security community’s historical preference for custom detectors¹ [19]–[21], [27], [56], [57] due to the complexity and heterogeneity of provenance graphs, we chose a general GNN framework for universal applicability and broader impact. Notably, the DGL community has integrated our heterogeneous GNN enhancement [59]–[63].

2.3. Explainability and Security Applications

Explaining ML-based Security Models. Due to the importance of explainability in the security domain, several explainers have been proposed different explainability framework for ML-based security analysis. LEMNA [64] focused on classifying PDF malware and detecting a function’s entry point in binary code using regression mixture models as a localized surrogate to approximate the classifier’s decision boundary. Recent works such as CFGExplainer [65] and FC-GAT [66] use deep surrogate models to explain GNN-based malware detection using control flow graphs and function call graphs, respectively. These methods exclusively work on homogeneous graphs, thus cannot be directly applied to heterogeneous provenance graphs.

Jacob et al. [67] proposed TRUSTEE, a framework that generates decision tree (DT)-based interpretations for ML models to detect shortcut learning (*e.g.*, problem under-specification). Their success clarifying model decisions about network packets inspired us to generalize the approach to the system provenance domain. The core challenge is that the system provenance domain relies on heterogeneous multi-attributed graph datasets, which are not natively consumed by DTs. By focusing solely on graph structure and leveraging security-oriented graph structural features, PROVEXPLAINER enables DT-based explanations in the provenance domain.

Explaining GNN Models. Recent research in GNN explainers [28]–[30] has advanced in identifying key nodes, edges, or subgraphs in GNNs, and are categorized into white-box

1. It has only been recently that GNNs have started gaining attention within the community.

and black-box explainers. White-box methods, *e.g.*, GNNExplainer [28] and PGExplainer [29], access GNN internals, including model weights and gradients. Conversely, black-box methods like SubgraphX [30] operate on model inputs and outputs, reducing coupling between the explanation framework and model architecture. [68] has shown high variance in explanations provided by traditional GNN explainers, raising reliability and applicability concerns.

2.4. Ground-truth Verification

Ground truth verification of ML model decisions in security-critical tasks has garnered significant attention, underscoring the role of explanations in unveiling the truth [31]–[33]. These studies highlight the effectiveness of white-box techniques in malware detection and vulnerability discovery, with further advancements in reconstructing ground truth around local explanations [33].

In system provenance, “ground truth” refers to the real-world information against which the validity of a model’s predictions are checked. In this paper, we approximate the ground truth using documentation created by security vendors, tech reports, and previous studies. The relevant processes, files, and network sockets mentioned in the documentation are designated as *documented entities*. We understand that the documentation provided by the security vendors can have experimental errors, as well as selection and experimental bias. To mitigate these problems, we aggregated information from multiple sources. We extract *documented entities* with three methods: (1) referring to pre-existing malware profile databases that contain information from different security vendors, such as VirusTotal [51], we obtain activity summaries detailing network communications, file system actions, and process behaviors; (2) we extract key entities (*i.e.*, process involved, files created and connections made) from tech reports [69], [70] and system manuals [71]; (3) we consult dataset authors [46] and review dataset documentation to identify the components of each attack present in the datasets.

3. Problem Statement and Threat Model

Our research addresses explainability in GNN-based security models built on system provenance graphs, tackling a core issue in the security domain. The complexity of explaining GNN decisions is exacerbated by graph structural learning, which adds to the inherent complexity of Neural Networks (NNs). Existing studies on GNN explainability [28]–[30], [33], [65], [72] often fail to effectively map back to system behaviors in the provenance domain. To bridge this gap, our framework employs a surrogate DT-based method that utilizes interpretable security-aware graph structural features (*i.e.*, discriminant subgraph patterns and graph structural features) to explain GNN decisions. A graph explanation method \mathcal{E} will yield a total ordering over \mathcal{V} for a given graph $\mathcal{G} = (\mathcal{V}, \mathcal{E})$ and graph model \mathcal{M} .

Our threat model assumes the integrity of on-device data collection, relying on provenance records secured by

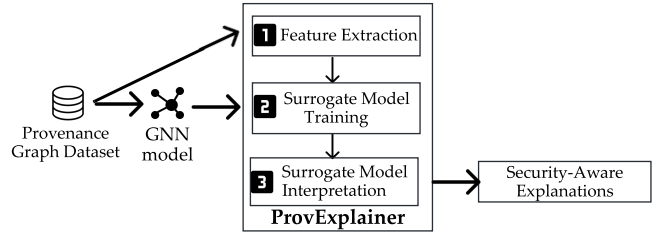


Figure 1: PROVEXPLAINER architecture.

existing mechanisms ([15], [18]–[21], [46], [73], [74]). Our primary objective is to generate security-aware explanations to aid security analyst and increase their trust in the GNN’s decisions. We consider graph-level anomaly detection tasks; explaining GNN decisions in node/edge level tasks is outside the scope of this work. Systematically aggregating an accurate and trustworthy ground truth for malware and APT behaviors pose a challenging open problem. In this paper, we approximate the ground truth using publicly available documentation (§2.4). In line with recent literature on GNN explanation [31], [32], [65], adversarial samples are outside the scope of the paper. Creating robust detection and explanation systems that can withstand adversarial manipulation [46], [75], procedural dataset poisoning, and detection model manipulate are critical open research problems that are orthogonal to our work.

4. PROVEXPLAINER Overview

We apply PROVEXPLAINER in three stages (Figure 1).

Stage 1: Extract Security-aware Features (§4.1). We extract security-relevant subgraph patterns using a discriminative subgraph mining approach and graph structural features that facilitate distinction between benign and anomalous datasets. These subgraph patterns enable the identification of localized attack vectors, while global structural features capture holistic structural changes.

Stage 2: Train an Interpretable Surrogate Model (§4.2). Next, we utilize diverse system provenance dataset to train an interpretable surrogate DT that aligns with the GNN decisions using the extracted features. Since the GNN’s decision-making process relies on a structure-dependent message-passing algorithm, we efficiently mimic the decision-making process of the GNN’s using the structure-based features.

Stage 3: Interpret the Surrogate Model (4.3). To extract the explanation for a detection using the surrogate DT, we extract the graph nodes participating in the subgraph patterns that contribute to the DT’s decision. These explanations are valid only when the surrogate agrees with the GNN.

4.1. Feature Extraction

4.1.1. Subgraph Features. The extraction of subgraph features is pivotal in distinguishing anomalous patterns from benign patterns within provenance datasets. To avoid information leakage and ensure no data snooping, patterns

Algorithm 1 Discriminative Pattern Mining

Require: Subgraph patterns, subgraph pattern sizes, subgraph pattern support, and K to select the top K
Ensure: Discriminative subgraph patterns

- 1: Aggregate subgraphs for anomaly and benign datasets in training set
- 2: Calculate coverage and diversity for each pattern
- 3: Assign scores using for each pattern based on diversity (div), coverage (cov), pattern size (size), and pattern support (support):
$$\text{Score} = \alpha \cdot \text{div} + \beta \cdot \text{cov} + \gamma \cdot \text{size} + \eta \cdot \text{support}$$
- 4: Compute score difference for each pattern between benign and anomaly datasets
- 5: Select top- K patterns with largest score differences using `argmax_pattern`
- 6: Save selected features and associated scores

are mined exclusively on the training dataset, with a clear separation between training and testing data. This approach enables unbiased pattern discovery and allows the identified discriminative features to be evaluated solely on the testing dataset, maintaining a rigorous evaluation protocol.

Each file in the training dataset undergoes frequent subgraph pattern mining using a graph evolution miner (GERM [37]), where subgraphs of specified *pattern sizes* and *support* thresholds are identified. Support means how many of the subgraph instances were identified in the graph. As described in **Algorithm 1**, from each file, subgraphs are extracted based on structural pattern, generating unique patterns termed *subgraph keys*. These keys serve as representative features, capturing the frequency and structure of motifs present in the datasets.

For each subgraph pattern, we calculate its *pattern diversity*, which measures the structural complexity of the pattern. Diversity scores are computed by aggregating node and edge weights, where node weights are assigned according to unique node labels, and edge weights reflect the types of connections between nodes. This diversity score quantifies the variability within each pattern, aiding in highlighting complex, potentially discriminative structures.

We also measure the *coverage* of a subgraph pattern by measuring its presence across files within the dataset, providing a statistical representation of how commonly the pattern occurs in the dataset as a whole. Calculated as the proportion of files in which the pattern appears with non-zero support, coverage serves as an indicator of the pattern's prevalence or rarity in benign and anomalous instances. High coverage patterns suggest commonly occurring structures within the respective dataset, representing anomalous or benign operations. We want to identify patterns that have high coverage in anomalous but low coverage in benign datasets, providing a basis for distinguishing between them.

By incorporating coverage into the scoring function, we ensure that patterns contributing significantly to the anomalous dataset's structure are prioritized, enhancing the model's ability to generalize from typical behaviors to rare distinctive malicious behavior, indicative patterns. To quan-

tify the discriminative utility of each pattern, we define a *scoring function* parameterized by weights α, β, γ , and η , which represent the relative importance of diversity, coverage, pattern size, and support, respectively. The scoring function is formulated as follows:

$$\text{Score} = \alpha \cdot \text{div} + \beta \cdot \text{cov} + \gamma \cdot \text{size} + \eta \cdot \text{support}$$

where div denotes the calculated diversity of the pattern, cov represents the proportion of files in which the pattern appears, size is the average number of nodes in the pattern, and support reflects the frequency of occurrence of the pattern within each file. For our study, we used the following hyperparameters: $\alpha = 0.2$, $\beta = 0.4$, $\gamma = 0.1$, and $\eta = 0.3$. These values were selected to prioritize coverage and support as the primary differentiators, while also ensuring that the extracted patterns are diverse and large in size, in that order of importance.

The scoring function is applied separately to the benign and anomaly datasets in the training set. Patterns that maximize the absolute score difference between benign and anomaly datasets are selected as discriminative patterns, as they are likely to differentiate between benign and anomalous behaviors effectively. The top k patterns with the largest score differences are retained and subsequently evaluated on the testing dataset, thus ensuring that the pattern discovery and evaluation are conducted independently.

4.1.2. Graph Structural Features. From graph theory literature, we selected the following structural features [76]: degree centrality, closeness centrality, betweenness centrality, eigenvector centrality, clustering coefficient, and clustering triangles. These standard features are known for capturing the key characteristics of graphs, serving as a custom signature that effectively reflects the global properties of a graph. To refresh the reader, we provide informal definitions of each feature and what is the expected trend in system graphs.

Degree Centrality. Degree centrality is simply the degree of the node, or the count of its incident edges. The degree centrality of a node indicates the extent of its direct connections in the graph. When aggregated across all nodes, high degree centrality values suggest a densely connected system with significant interactivity, whereas low values indicate sparsely connected regions, potentially reflecting isolated or specialized nodes. High degree centrality could suggest the presence of core process hubs, while low values imply a more dispersed system with no central process hubs. However, degree centrality alone cannot definitively indicate malicious behavior. For example, a long-running attack creating a long process chain show low degree centrality, while attacks that interact with many files or fork multiple child malware processes will exhibit high degree centrality. In the case of a cryptominer masquerading as `schtasks.exe`, we would expect the benign `schtasks.exe` to show low centrality as it merely schedules tasks, while the cryptominer malware would have high centrality due to spawning multiple malicious processes.

Closeness Centrality. Closeness centrality is the inverse of the mean shortest path distance from all other nodes to the target node, indicating how close the node is within the graph. Closeness centrality measures how centrally located a node is within the graph by examining its proximity to other nodes. High closeness centrality across the graph suggests that many nodes are relatively close to each other, indicating efficient communication pathways. In contrast, low closeness centrality values highlight dispersed sections of the graph, potentially representing decentralized or peripheral interactions within the system. High closeness centrality indicates well-connected process hubs central to the system, while low values suggest that processes are widely dispersed with limited central hubs. Empirically, system processes often have high closeness centrality, while user-level or malware processes show lower values. For instance, botnets masquerading as system-level processes will be distinguishable, since botnet will have a higher closeness centrality due to multiple network connecting being created characteristic of their DDoS activities.

Betweenness Centrality. Betweenness centrality measures the frequency with which a node appears on the shortest paths between other nodes, highlighting its role as a waypoint. It indicates how often a node acts as a bridge along the shortest paths between other nodes. High betweenness centrality suggests a system’s reliance on certain core hubs or bottleneck paths, while lower values indicate multiple alternative pathways and a more distributed structure. High betweenness centrality indicate processes that serve as intermediaries in data or control flow, whereas low values suggest a network of distributed pathways with minimal reliance on specific process hubs. Malware like worms and spyware tend to have low betweenness centrality, as they seek to spread across the system and create multiple information pathways without centralizing the flow.

Eigenvector Centrality. Eigenvector centrality assigns higher values to nodes connected to other influential nodes, reflecting the prominence of node clusters that are influential. High eigenvector centrality in processes indicates hubs with extensive control over information flow, while low values imply a flatter structure without prominent hubs. Ransomware tends to have high eigenvector centrality, as malicious processes involved in reading and encrypting files act as critical nodes. By keeping few child processes, ransomware conserves system resources, allowing high-volume file encryption without overloading the system.

Clustering Triangles. Clustering triangles count the number of triangles that include the node. The clustering triangles count represents the frequency of triangular connections in the graph. High clustering triangle values indicate localized connectivity, suggesting shared resources or close interactions among nodes, while low values indicate a more hierarchical or linear flow. Malware often creates prominent triangles when, for example, they write template files and repeatedly execute them, making copies of themselves. Similarly, legitimate programs like `svchost.exe` (a service scheduler) may form triangles when creating `conhost.exe`

and reading common `*.dll` files. In contrast, ransomware typically reads files to encrypt them, forming a “spoke-and-wheel” shape rather than triangles, resulting in lower triangle counts than benign processes like `svchost.exe`.

Clustering Coefficient. The clustering coefficient is calculated by dividing the number of triangles the node participates in by its degree, indicating how close its connections form a complete graph with its neighbors. The clustering coefficient measures the degree to which nodes’ neighbors are interconnected. A high clustering coefficient suggests that nodes form close-knit groups, often indicating shared resources or community-like interactions, while a low coefficient reflects more dispersed connections. High clustering coefficients point to strong groupings around key processes with shared resources, while low values suggest processes with less close-knit hubs. The clustering coefficient provides a similar interpretation to closeness centrality; however, while closeness centrality highlights a process’s accessibility within the system, the clustering coefficient emphasizes the density of its immediate neighborhood connections.

4.2. Surrogate Model Training

To obtain explanations from our security-aware graph structural features, we use them to train a global surrogate DT. By training a DT to agree with the predictions of a GNN model, we can interpret the DT to gain insights about the GNN’s decision-making process. To achieve the best agreement results, we enhance traditional DT training with data augmentation that iteratively increases the weight of incorrectly classified samples [67].

We begin with a labelled set of graphs $D_G = (G, Y)$, which is used to train the GNN. GNN’s predictions on D_G are collected, yielding $GNN(D_G) = Y'$. To prepare the dataset for training the DT, we extract the discriminative subgraph patterns and graph structural features (§4.1) F and associate them with the GNN’s predictions Y' to create a labelled feature dataset $D_F = (F, Y')$, which we split into train, validation, and testing to evaluate the surrogate DT.

Leveraging the methods of Jacobs et al. [67], we use two-layer iterative dataset augmentation to train a series of DT models. At each iteration of the inner loop, all misclassified samples are duplicated to increase their weight in the next iteration; from this series of models, we select the one with the highest agreement among the DTs. This process is repeated several times in the outer loop, then the surrogate model with the highest mean agreement among those high-agreement DTs is selected as the final surrogate model for explanation.

4.3. Surrogate Model Interpretation

Once the surrogate DT is trained, we get instance-level explanation as it not only enables explanations based on local subgraph structures but also global structural changes. Each decision node within the DT represents a subgraph structure or a graph structural measure along with its threshold. Decision nodes closer to the root of the DT exert the

greatest influence on the decision path; thus, we rank the nodes that participate in subgraphs based on their relative positioning in the decision tree. In cases where the decision path contains only graph structural measures without subgraph patterns, node-level explanations cannot be extractable, even if a DT tree is generated. While structural metrics alone face challenges in pinpointing specific nodes, they remain essential indicators of long-running persistent APT attacks. During an APT attack, though determined attackers may preserve node-level attributes, they typically cannot preserve benign program’s graph structure. Another scenario where explanations is invalid is when the surrogate model’s prediction disagrees with the GNN’s prediction.

System attributes (*e.g.*, process/file names and socket IP/port) can be extracted in a post-processing step. Finally, the interpretable surrogate DT facilitates the construction of actionable, security-aware explanations for individual decisions. Since PROVEXPLAINER produces a global surrogate DT, domain experts can use it to deepen their understanding of the GNN’s decision-making process. In our experiments, we found that limiting DT nodes to a depth of 4 provided the most effective explanations in our datasets. Lower depths failed to capture shapes needed for complex APT scenarios, while higher depths introduced irrelevant system behaviors. Due to the DT’s susceptibility to overfitting, restricting the depth was necessary.

5. Evaluation

In this section, we evaluate PROVEXPLAINER’s effectiveness in explaining stealthy attacks. We aim to answer the following research questions (RQs):

RQ1: Explanation Accuracy. Can PROVEXPLAINER explain APT and Fileless malware detection ([§5.3, §5.4](#))?

RQ2: Comparison with SOTA GNN Explainers. How do the explanations of PROVEXPLAINER compare against those of SOTA GNN explainers (GNNExplainer [\[28\]](#), PGExplainer [\[29\]](#), and SubgraphX [\[30\]](#)) ([§5.5](#))?

5.1. Evaluation Protocols

We evaluate PROVEXPLAINER against different APT detection datasets and Fileless Malware datasets: (1) publicly available APT attack simulations [\[45\]](#), (2) APT dataset from a recent study [\[46\]](#), and (3) execution traces of Fileless Malware [\[47\]](#). We implemented two general purpose SOTA GNN-based detector models: GAT [\[77\]](#) and GraphSAGE [\[78\]](#), following the approach of recent explanation literature [\[65\], \[68\]](#). Recent GNN based anomaly detection systems [\[19\]–\[21\], \[27\], \[57\]](#) rely on custom node and edge embeddings for security tasks and they do not use the GNN for anomaly detection task but rather use them for extracting graph embeddings and use another downstream model for anomaly detection, so we did not evaluate against these specialized solutions.

We conducted an ablation study to understand the impact of different feature sets consisting of subgraph patterns and

graph structural features. Finally, we evaluated the explanations given by PROVEXPLAINER against those of SOTA GNN explainers [\[28\]–\[30\]](#) In [§6](#), we present case studies highlighting specific instances of APT detection and offer in-depth insights into how our approach provides security relevant explanations.

Evaluation Metrics. In our evaluation of PROVEXPLAINER, we focus on three critical aspects. The first is the agreement of the surrogate DTs with the GNN model, which we measure using the weighted macro averaged (WMA) F1 score of the surrogate DT’s predictions with respect to the GNN’s predictions. The *agreement* metric gauges the faithfulness of the DT in replicating the conclusions of GNNs. The choice of the WMA F1 score accounts for the data imbalance issue in the anomaly detection datasets.

The second metric is fidelity^+ and fidelity^- used by different GNN explainers [\[72\]](#) which measures if we remove the important subgraph pattern does the class label flip and if we remove unimportant subgraph patterns the class label should not change. A good explainer is the one that will have a high fidelity^+ and a low fidelity^- .

To evaluate PROVEXPLAINER’s and SOTA GNN explainers’ proficiency in identifying security-relevant entities, we define precision and recall metrics with respect to documented entities [§2.4](#). A graph explanation method \mathcal{E} will yield a total ordering over \mathcal{V} for a given graph $\mathcal{G} = (\mathcal{V}, \mathcal{E})$ and graph model \mathcal{M} . Let \mathcal{D} be the set of documented entities. *Precision* is the proportion of explanation nodes that are documented, and *recall* is the fraction of documented entities retrieved: $\text{precision}(V_k, k, \mathcal{D}) = \frac{|V_k \cap \mathcal{D}|}{k}$, and $\text{recall}(V_k, \mathcal{D}) = \frac{|V_k \cap \mathcal{D}|}{|\mathcal{D}|}$.

5.2. Evaluation Tasks

APT Detection. We utilized the DARPA Transparent Computing (TC) Data Releases [\[45\]](#) and previous literature [\[46\]](#) for APT attack detection. This dataset, encompassing various OSes, provides a comprehensive basis for advanced security research. The DARPA APTs were designed to attack a system which consists of long-running processes and captured the stealthy attack vectors frequently employed by advanced adversaries. We particularly focused on three DARPA datasets used by previous studies [\[19\]–\[21\], \[57\]](#): FiveDirections, Trace, and Theia. However, these tasks were conducted in a simulated environment and only lasted for two weeks, involving a limited number of hosts. Therefore, we also evaluated against the APT scenarios (*e.g.*, Enterprise APT and Supply-Chain APT) conducted by [\[46\]](#), which were performed with realistic benign background workloads. Interested readers can find detailed statistics presented in [Table 4](#) in the appendix.

Fileless Malware Detection. For Fileless Malware detection, we targeted a family of stealthy malware samples that impersonate benign programs, evading conventional security solutions but are detectable by GNN-based provenance analysis. The malware samples were chosen in accordance with guidelines from the literature [\[79\], \[80\]](#) to minimize ex-

TABLE 2: Surrogate DTs have high agreement (≥ 0.85) with the decisions of GNN measured using the WMA F1 score.

Dataset	GAT	Surrogate DT (agree w/ GAT)	GraphSAGE	Surrogate DT (agree w/ GraphSAGE)
APT Dataset from [46]				
Enterprise Supply-Chain	0.82	0.95	0.81	0.94
Enterprise Supply-Chain	0.82	0.94	0.80	0.97
Average	0.82	0.95	0.81	0.95
DARPA APT Dataset [45]				
FiveDirections	0.82	0.88	0.82	0.85
Trace	0.93	0.93	0.87	0.87
Theia	1.00	1.00	0.94	0.94
Average	0.92	0.93	0.88	0.89
Fileless Malware from [47]				
wscript.exe	1.00	1.00	0.95	0.95
cscript.exe	1.00	1.00	1.00	1.00
reg.exe	1.00	1.00	1.00	1.00
python.exe	0.99	0.99	0.99	0.99
explorer.exe	0.98	0.98	1.00	0.98
netsh.exe	0.98	0.98	0.98	0.98
net.exe	0.97	0.97	0.97	0.97
rundll32.exe	0.96	0.96	0.96	0.96
mshta.exe	0.95	0.95	0.85	0.85
schtasks.exe	0.93	1.00	0.93	1.00
conhost.exe	0.89	0.89	0.93	0.93
svchost.exe	0.86	1.00	0.86	1.00
Average	0.96	0.98	0.95	0.97

perimental bias and ensure freshness. The Fileless Malware dataset includes various categories [79], including banking Trojans, spyware, ransomware, and malware installers; detailed statistics presented in Table 4 in the appendix.

The Banking banking trojan [79] steals banking credentials from victim machines and spreads through spam and compromised download links. To camouflage interactions with .dlls and temporary files, it masquerades as `svchost.exe`. The Spyware, Ulise [79], is a multi-purpose Trojan that can establish remote access connections, capture keyboard input, collect system information, download/upload files, drop other malware into the infected system, and perform encryption. Because it propagates through the network sockets and interacts with many system files, it masquerades as `python.exe` as it needs a target that exhibits diverse behavioral patterns.

5.3. Graph Structural Feature Evaluation

To answer **RQ1**, Table 2 demonstrates the effectiveness of surrogate DTs in mirroring the decision process of GNN models like GAT and GraphSAGE. Agreement between the surrogate DT and the GNN is an important metric for two reasons: (1) surrogate explanations are only valid when the surrogate agrees with the GNN, and (2) high agreement indicates that the surrogate model is a good approximation of the GNN’s decision-making process.

PROVEXPLAINER exhibits the highest agreement ($> 97\%$) with the GNN models on the Fileless Malware datasets, but the APT datasets only showed good agreement ($> 93\%$). The surrogate DTs’ superior performance in Fileless Malware datasets can be attributed to PROVEXPLAINER’s ability to capture local subgraph patterns with high efficiency but APT attacks that are long running and utilize evasive tactics (noted by previous studies [46], [47]) are hard to detect and explain. The dataset

such as FiveDirections and `conhost.exe` are dominated by attackers using stealthy techniques such as *living-off-the-land*, which involve memory object interactions which are currently not captured in our provenance graphs. The absence of the distinguishing features impairs the effectiveness of PROVEXPLAINER.

We observed that GAT outperforms GraphSAGE in majority of the datasets. This trend is attributed to GAT’s ability to assign varying importance to different neighborhood structures and capture long-range structural dependencies through its attention mechanism. Conversely, GraphSAGE, which samples a fixed-size neighborhood, overlooks subtle structural changes, such as those resulting from elusive APT attacks. PROVEXPLAINER’s graph structural features enable surrogate DTs to efficiently approximate GNN models’ decision-making process on in-distribution data. Although the current features are sensitive to attacker’s TTP, PROVEXPLAINER is expandable to incorporate additional features to extend support to for new TTP explanation.

5.4. Ablation Study

Table 3 shows the contributions of different features to the overall agreement of surrogate DTs approximating a GAT model. Interested readers may find this study with GraphSAGE in the appendix, Table 5. We separate the features in two groups, subgraphs and graph structural features. We evaluate each group individually and then we look at the their combined effect. We further separate the group into individual features and look at the effect of each constituting features in the group. In the subgraph group, we use the top- K subgraphs as features, considering each of them one by one, then followed by using all top- K subgraphs. Second, we evaluate different graph structural features individually and then collectively.

The top- K subgraphs demonstrate varying levels of agreement across the datasets, in the APT dataset, we consider each of the top-5 subgraphs individually shows different level of agreement for both Enterprise and Supply-Chain dataset, indicating that different subgraphs captures different signals in the graph to explain, therefore the alignment with the original model predictions stays constant. The trend is similar for the DARPA TC and Fileless Malware datasets, although the increase in agreement levels tends to plateau as K approaches 4, suggesting that the initial few subgraphs capture the majority of informative patterns. Dissimilar to subgraph patterns when we examining individual structural features the performance varies significantly depending on the feature used. For instance, eigenvector centrality and clustering coefficient consistently shows higher agreement in the DARPA TC dataset, particularly in Trace and Theia both achieving agreement scores of 1.00. In contrast, closeness and betweenness centrality features are comparatively lower in agreement for most datasets, possibly indicating that these features does not capture unique graph characteristics that are distinguishable.

Combining the top-5 subgraphs and all structural features generally results in high alignment with the model,

TABLE 3: Agreement (higher is better) measured using WMA F1 score of surrogate DTs with the GAT model across different features.

Dataset	Top- K Subgraphs					All Top 5 Subgraphs	Graph Structural Features					All Graph Structural Feat.	All Features	
	1	2	3	4	5		Deg. Cen.	Clos. Cen.	Bet. Cen.	Eig. Cen.	Clus. Coeff.	Clus. Tri.		
APT Dataset from [46]														
Enterprise Supply-Chain	0.90 (-.05)	0.90 (-.05)	0.90 (-.05)	0.90 (-.05)	0.90 (-.05)	0.92 (-.03)	0.92 (-.03)	0.92 (-.03)	0.92 (-.03)	0.95 (-.00)	0.95 (-.00)	0.82 (-.13)	0.95	
Average	0.79 (-.16)	0.85 (-.09)	0.86 (-.08)	0.87 (-.07)	0.87 (-.07)	0.93 (-.01)	0.93 (-.01)	0.93 (-.01)	0.94 (-.00)	0.94 (-.00)	0.94 (-.00)	0.82 (-.12)	0.94	
DARPA APT Dataset [45]														
FiveDirections	0.72 (-.16)	0.75 (-.13)	0.75 (-.13)	0.72 (-.16)	0.72 (-.16)	0.72 (-.16)	0.72 (-.16)	0.72 (-.16)	0.78 (-.10)	0.78 (-.10)	0.78 (-.10)	0.84 (-.04)	0.86 (-.02)	0.88
Trace	0.93 (-.00)	0.93 (-.00)	0.93 (-.00)	0.93 (-.00)	0.93 (-.00)	0.87 (-.07)	0.87 (-.07)	0.87 (-.07)	0.87 (-.07)	0.93 (-.00)	0.93 (-.00)	0.93 (-.00)	0.93 (-.00)	0.93
Theia	0.83 (-.17)	0.83 (-.17)	0.89 (-.11)	0.89 (-.11)	0.89 (-.11)	0.89 (-.11)	1.00 (-.00)	1.00 (-.00)	1.00 (-.00)	1.00 (-.00)	1.00 (-.00)	1.00 (-.00)	1.00 (-.00)	1.00
Average	0.84 (-.10)	0.88 (-.07)	0.88 (-.07)	0.89 (-.06)	0.89 (-.06)	0.93 (-.02)	0.93 (-.02)	0.93 (-.02)	0.95 (-.00)	0.95 (-.00)	0.95 (-.00)	0.82 (-.12)	0.95	
Fileless Malware from [47]														
wscript.exe	0.93 (-.07)	0.93 (-.07)	0.93 (-.07)	1.00 (-.00)	1.00 (-.00)	0.98 (-.02)	0.98 (-.02)	0.98 (-.02)	1.00 (-.00)	1.00 (-.00)	1.00 (-.00)	1.00 (-.00)	1.00 (-.00)	1.00
cscript.exe	0.86 (-.14)	0.86 (-.14)	0.93 (-.07)	0.93 (-.07)	1.00 (-.00)	1.00 (-.00)	1.00 (-.00)	1.00 (-.00)	1.00 (-.00)	1.00 (-.00)	1.00 (-.00)	1.00 (-.00)	1.00 (-.00)	1.00
reg.exe	0.92 (-.08)	0.92 (-.08)	0.92 (-.08)	0.92 (-.08)	0.92 (-.08)	0.92 (-.08)	0.92 (-.08)	0.92 (-.08)	1.00 (-.00)	1.00 (-.00)	1.00 (-.00)	1.00 (-.00)	1.00 (-.00)	1.00
python.exe	0.59 (-.41)	0.66 (-.34)	0.66 (-.34)	0.66 (-.33)	0.65 (-.35)	0.94 (-.06)	0.94 (-.06)	0.94 (-.06)	0.99 (-.00)	0.99 (-.00)	0.99 (-.00)	0.99 (-.00)	0.99 (-.00)	0.99
explore.exe	0.74 (-.25)	0.91 (-.07)	0.91 (-.07)	0.91 (-.07)	0.91 (-.07)	0.91 (-.07)	0.91 (-.07)	0.91 (-.07)	0.98 (-.00)	0.98 (-.00)	0.98 (-.00)	0.98 (-.00)	0.98 (-.00)	0.98
netsh.exe	0.93 (-.04)	0.91 (-.07)	0.91 (-.07)	0.91 (-.07)	0.91 (-.07)	0.91 (-.07)	0.91 (-.07)	0.91 (-.07)	0.98 (-.00)	0.98 (-.00)	0.98 (-.00)	0.98 (-.00)	0.98 (-.00)	0.98
net.exe	0.94 (-.02)	0.94 (-.02)	0.94 (-.02)	0.94 (-.02)	0.94 (-.02)	0.91 (-.06)	0.91 (-.06)	0.91 (-.06)	0.97 (-.00)	0.97 (-.00)	0.97 (-.00)	0.97 (-.00)	0.97 (-.00)	0.97
rundll32.exe	0.85 (-.10)	0.85 (-.10)	0.85 (-.10)	0.85 (-.10)	0.85 (-.10)	0.85 (-.10)	0.85 (-.10)	0.85 (-.10)	0.96 (-.00)	0.96 (-.00)	0.96 (-.00)	0.96 (-.00)	0.96 (-.00)	0.96
mshta.exe	0.75 (-.20)	0.75 (-.20)	0.75 (-.20)	0.75 (-.20)	0.75 (-.20)	0.90 (-.05)	0.90 (-.05)	0.90 (-.05)	0.95 (-.00)	0.95 (-.00)	0.95 (-.00)	0.95 (-.00)	0.95 (-.00)	0.95
schtasks.exe	0.98 (-.02)	0.98 (-.02)	0.98 (-.02)	0.98 (-.02)	0.98 (-.02)	0.98 (-.02)	0.98 (-.02)	0.98 (-.02)	1.00 (-.00)	1.00 (-.00)	1.00 (-.00)	1.00 (-.00)	1.00 (-.00)	1.00
conhost.exe	0.91 (-.02)	0.89 (-.00)	0.89 (-.00)	0.89 (-.00)	0.89 (-.00)	0.93 (-.04)	0.93 (-.04)	0.93 (-.04)	0.89 (-.00)	0.89 (-.00)	0.89 (-.00)	0.89 (-.00)	0.89 (-.00)	0.89
svchost.exe	0.98 (-.02)	0.98 (-.02)	0.98 (-.02)	0.98 (-.02)	0.98 (-.02)	0.98 (-.02)	0.98 (-.02)	0.98 (-.02)	1.00 (-.00)	1.00 (-.00)	1.00 (-.00)	1.00 (-.00)	1.00 (-.00)	1.00
Average	0.86 (-.11)	0.88 (-.09)	0.89 (-.09)	0.89 (-.08)	0.90 (-.08)	0.93 (-.05)	0.93 (-.04)	0.93 (-.04)	0.98 (-.00)	0.98 (-.00)	0.98 (-.00)	0.98 (-.00)	0.96 (-.02)	0.98

achieving around 0.94 in agreement for Fileless Malware datasets. An interesting pattern is that the Fileless Malware dataset consistently performs exceptionally well, particularly with individual features like eigenvector centrality and clustering triangles, which achieve near-perfect alignment scores. This suggests that the structural properties in the Fileless Malware dataset are distinctively different compared to their benign programs they are masquerading. In APT dataset where the attacker uses stealthy techniques more holistic feature combinations are needed for optimal performance. This trend suggests that when subgraph structures are combined with centrality and clustering metrics, they can capture a comprehensive representation of the graph structure, effectively enhancing the model’s agreement. The high performance across all datasets with this combination indicates that a more holistic representation of both the subgraph and graph structural features offers better alignment than individual metrics.

5.5. PROVEXPLAINER vs. SOTA Explainers

To answer **RQ2**, Figure 2 compares the fidelity⁺ and fidelity⁻, and Figure 3 compares the precision and recall of the explanations derived from SOTA methods (GNNExplainer, PGExplainer, and SubgraphX) with those derived from PROVEXPLAINER. Later, we will analyze specific case studies in §6.

fidelity⁺ and fidelity⁻. In the APT dataset from [46], ProvExplainer performs competitively for both fidelity⁺ and fidelity⁻. PROVEXPLAINER and SubgraphX have competitive fidelity⁺ performance and outperforming both GNNExplainer and PGExplainer. For fidelity⁻ ProvExplainer performs the best by having the lowest score after k=10 but interestingly SubgraphX performed the worst which leads to the conclusion that SubgraphX is not identifying all the important subgraph structures, so when we remove graph structure that SubgraphX deemed unimportant it is still changing the prediction that’s why in Figure 3 we can see it having the lowest recall value for GAT network.

PROVEXPLAINER was had the best performance across both fidelity types for DARPA TC dataset. In the DARPA and APT datasets, the security-aware features of PROVEXPLAINER provide a clear advantage in extracting important nodes from the provenance graphs whose removal changes the prediction, moreover low fidelity⁻ indicate that the GNN model is particularly identifying those security-aware features since if we remove any other part of the graph the prediction does not change. For Fileless Malware dataset PROVEXPLAINER’s performance is moderate for fidelity⁺. As we increased the size of k , PROVEXPLAINER became the best explainer but for the lower values of k , SubgraphX performed well. But similar to performance of APT dataset from [46] we saw that SubgraphX only focusing on some particular structures and not accounting for all the important substructures that are important for prediction as indicative of a high fidelity⁻.

Across all the datasets, PROVEXPLAINER shows an increase in fidelity values up to around $k = 25$. PROVEXPLAINER shows this improvement for fidelity⁺ across the APT datasets. Unfortunately, this trend also appears in fidelity⁻ but not much pronounced. This is because for long running and stealthy attacks, even the security-aware features are not enough, so it still missed some important graph structures that are important to the underlying GNN detection model. But, the increase of fidelity⁻ of other explainers are more rapid when compared to PROVEXPLAINER. Also, as k values are increased we see an inverse trend for fidelity⁺ and proportional trend for fidelity⁻, suggesting that when we either incorporate structures that produce unintended side effect and the label does not flip for fidelity⁺ and for fidelity⁻ we accidentally incorporate important subgraph structures whose removal changes the prediction.

Precision and Recall. In the APT dataset from [46], PROVEXPLAINER demonstrates competitive precision performance for both GAT and GraphSAGE networks compared to other GNN explainers, although it achieves comparatively high recall. This suggests that PROVEXPLAINER identi-

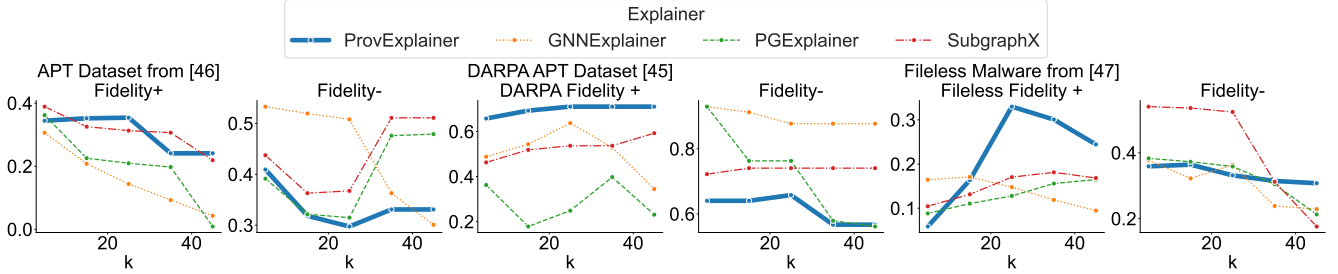


Figure 2: Effectiveness of GAT explainers in identifying prediction-relevant graph structures using fidelity⁺ (higher is better) and fidelity⁻ (lower is better).

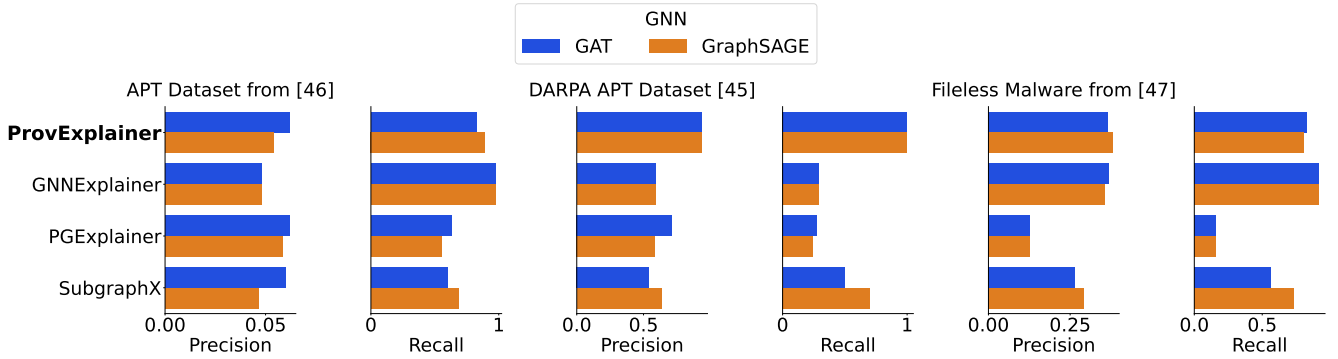


Figure 3: Effectiveness of GNN explainers at identifying documented entities, measured using precision and recall (higher is better for both).

fies more relevant instances, albeit at the cost of recall. In the DARPA TC dataset, PROVEXPLAINER significantly outperforms other explainers in both precision and recall, respectively, for both GAT and GraphSAGE networks. This indicates that PROVEXPLAINER is highly reliable in generating explanations for the APT datasets. In the Fileless Malware dataset category, PROVEXPLAINER achieves second best precision and recall, with values across GAT and GraphSAGE, respectively. GNNExplainer performs the well in this category, since Fileless Malware does not have intricate subgraph structures that are observed in APTs so GNNExplainer can identify them.

PROVEXPLAINER’s performance highlights a pattern of excelling in the APT datasets, where it achieves both high precision and perfect recall, suggesting a strong alignment with the characteristics and structure of this dataset. Meanwhile, its performance on the Fileless Malware dataset is moderate, and it has comparatively lower precision in the APT dataset from [46], where all explainers appear to face challenges. Regarding differences between GAT and GraphSAGE networks, PROVEXPLAINER exhibits consistently higher performance in both precision and recall across these networks within each category. Other explainers, such as SubgraphX, show an improvement in precision when using GraphSAGE, although differences in recall are less pronounced. This pattern suggests that GraphSAGE enhances the precision of some explainers without significantly impacting recall, although this effect is not uniform across all other SOTA explainers. GraphSAGE focuses on the

immediate neighbors of nodes, therefore it is less susceptible to irrelevant graph nodes.

A notable pattern emerges when comparing PROVEXPLAINER against other explainers across dataset. PROVEXPLAINER achieves high recall in the structured DARPA TC dataset, capturing relevant features more effectively than PGExplainer and GNNExplainer, which show much lower recall. Conversely, in the more complex APT dataset from [46], all explainers, including PROVEXPLAINER, struggle to achieve high precision, suggesting that the dataset’s complexity or feature overlap may limit their discriminatory power. In the Fileless Malware dataset, the generally high recall across explainers indicates their effectiveness in capturing indicative features, although precision remains challenging. These insights underscore PROVEXPLAINER’s strengths in structured datasets like DARPA TC and Fileless Malware and its limitations in more complex APT scenarios like APT dataset from [46], highlighting the influence of TTPs used by attackers on explainer performance.

6. Case Studies

To demonstrate PROVEXPLAINER in a realistic setting, we analyze three case studies from the DARPA [45] datasets. In each study, we use an explanation size of 40 nodes and refer to the GAT model. We list the most important features from the surrogate DT and qualitatively analyze the explanations from PROVEXPLAINER and the SOTA GNN

explainers. Detailed system-level analyses can be found in the appendix (§E).

6.1. FiveDirections: Browser Extension

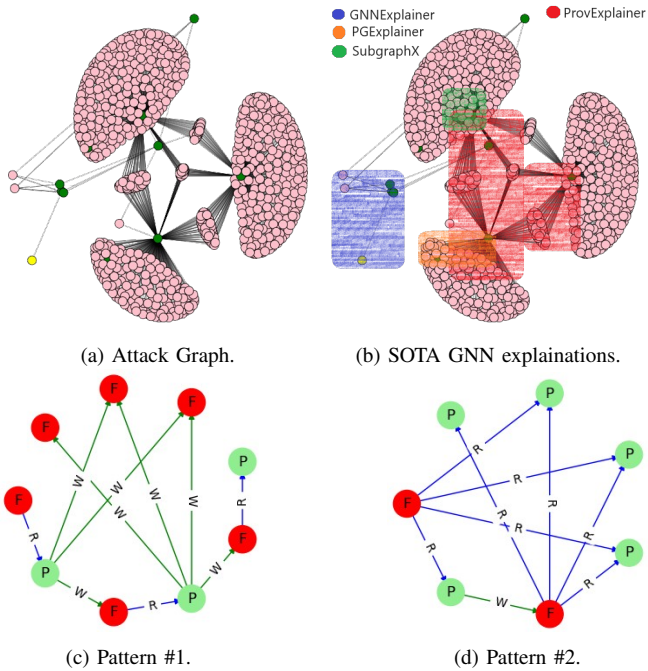


Figure 4: FiveDirections: the attacker exploits the target via a malicious Firefox extension.

Description. An attacker targets the Firefox browser using a malicious extension to deploy the drakon malware. The attacker writes drakon directly to disk and exploits a compromised browser extension masquerading as a password manager to execute malicious powershell code, gaining deeper access and control over the system, as illustrated in Figure 4.

Features: Degree centrality, pattern #1, and pattern #2.

System Interpretation. This attack graph contains the pattern #1 and pattern #2 in large numbers, which are often observed in the APT stages of *deepen access* and *lateral movement*. The pattern #1 is created when malwares have to transfer information among them selves. Therefore, after reading from a file, the malware updates the template and configuration files that other malwares in the system will read before executing their task. The pattern #2 is created since the malware in the system are copies therefore they need to read reads the same template files and .dll files as the original malware. Therefore, these patterns captures the dependency correlation among malware processes, where multiple instances of drakon exploit Firefox vulnerabilities via a malicious extension to spread to different parts of the system. This pattern is emblematic of malware processes cloning themselves to persist in the system as well as maintain operational integrity. Further, the pattern #2 highlights how malware processes move laterally to

exfiltrate sensitive data and read configuration files. Since the attack graph contains high quantities of file read and write flowers for a relative small number of nodes, it leads to a high degree centrality.

PROVEXPLAINER vs. SOTA explainers. Figure 4b compares the explanations of PROVEXPLAINER and those of SOTA GNN explainers, focusing on their efficacy in identifying security-aware elements. PROVEXPLAINER excels by highlighting the malware replicating itself from template files and accessing sensitive system files. PROVEXPLAINER isolates security-relevant structures in the graph, significantly increasing the end-user trust in the detection.

GNNExplainer identifies the malware template file and the malicious extension. This effectiveness stems from GNNExplainer’s method of searching for important edges. When this GNNExplainer isolates the pivot structure, the graph becomes disjoint, leading to a change in prediction. This results in a high information gain, the core metric for GNNExplainer. On the other hand, PGExplainer and SubgraphX reveal commonalities across attack graphs, such as the identification of key system library accesses required for malware operation. SubgraphX’s effectiveness varies due to its Monte Carlo Tree Search (MCTS), suggesting benefits to incorporating domain-specific insights into SubgraphX’s scoring function.

6.2. FiveDirections: Copykatz

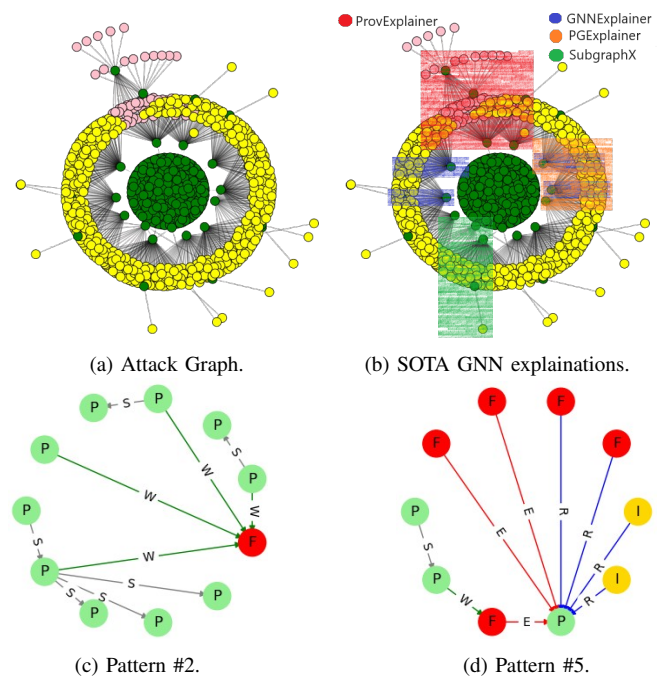


Figure 5: FiveDirections: the attacker gains C2 connections and installs Copykatz through a Firefox exploit.

Description. In a sophisticated attack, a hijacked version of usdoj.gov exploits Firefox to deploy drakon malware to

the victim host. Then, drakon uses the *elevate* driver to escalate privileges and masquerade as the *runtimebroker* system program. Finally, the malicious *runtimebroker* instance connects to a command and control (C2) server to download and execute *Copykatz* (an older version of *Mimikatz*) to harvest and exfiltrate host credentials, as illustrated in Figure 5.

Features: Degree centrality, pattern #2, and pattern #5.

System Interpretation. The attack graph highlights high degree centrality and two key patterns: #2 and #5. The pattern #2 captures the initial access by starting multiple malicious processes and writing to template files. The template files are written to by other malware child processes. This stage enables the Windows Application Programming Interface and cryptographic operations necessary for the malware’s functionality. Following this, the malware disguises itself as *Firefox*, and executes the *Copykatz* payload.

The malicious *Firefox* instance then distributes its payload through writing to temporary files, setting the stage for a subsequent malicious *Firefox* instance to trigger a flood of sensitive file reads and making network connections. This chain of actions, marked by inherited functionalities from *Copykatz*, forms the pattern #5. The replication of this malware leverages the same essential system libraries, indicating a meticulous design to maintain operational consistency throughout the malicious process chain. Similarly to the previous case study, due to high volume of network connections and processes creation the degree centrality is very high for the attack graph.

PROVEXPLAINER vs. SOTA explainers. GNNExplainer and PGExplainer pinpoint the stage where multiple *Firefox* processes connect to the C2 servers. This activity traces back to the malicious *runtimebroker* instance. Notably, SubgraphX detects an alternate trajectory where a *Firefox* process, instead of reaching out to external servers, spawns another process aimed at local content manipulation, showcasing the malware’s versatility in engaging with both external and internal resources for its objectives.

While SOTA explainers have demonstrated proficiency in identifying the final stages of this data breach, only PROVEXPLAINER effectively captured both the initial infection and its propagation. This distinction underscores the importance of recognizing early-stage indicators for root cause analysis.

6.3. Trace: Phishing E-mail

Description. The attacker first launches a phishing campaign to compromise the identity of an employee. Leveraging the employee’s identity, the attacker then targets other employees with deceptive emails containing links to a malicious website. This website installs a Trojan in the victims’ computers, which then creates multiple copies of itself, overflowing the system. These cloned Trojans read sensitive user files while the original Trojan achieves persistence in the system, as illustrated in Figure 6.

Features: Clustering coefficient, pattern #1 and pattern #2.

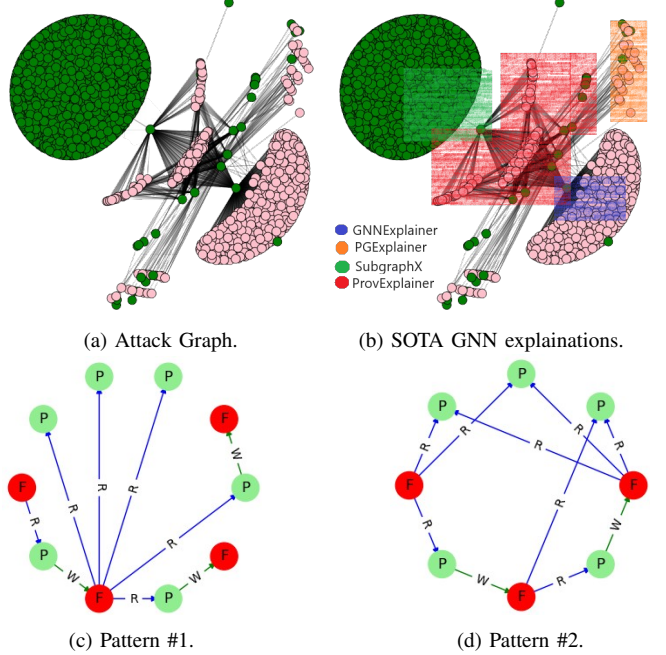


Figure 6: Trace: after an employee clicks on a phishing link, Firefox installs multiple Trojans to exfiltrate sensitive data.

System Interpretation. In the Trace APT scenario, clustering coefficient, pattern #1 and pattern #2 elucidate the malware’s structure. Pattern #2 reveals the Trojan’s propagating activity, where it reads from template files and prepares to replicate itself to establish a foothold. By masquerading as benign programs, the malware disguises its malicious processes, allowing it to proliferate undetected. The clustering coefficient of the graph increases because of multiple malware reading the template files by forming large process creation and file read clusters.

The Trojan, after establishing itself, impersonates system processes to write a malicious script, leading to other malicious process reading that script as seen in pattern #1. It illustrates the dependency correlation among the cloned malware instances, interacting with similar system configuration files to operate efficiently as well as constructing a detailed profile of the target system. Ultimately, a series of intra-malware communication happens where the malware reads from script and write to a file, and other malware update the script based on the current configuration. So, that the subsequent malware that read from the file gets the updated configuration.

PROVEXPLAINER vs. SOTA explainers. GNNExplainer identifies the initial malware staging behaviors, including interactions with shared libraries and cache files. Meanwhile, PGExplainer captures the benign structure of *xfce4-appfinder*—a lightweight desktop environment for UNIX systems, invoked by a DARPA script to simulate an enterprise environment. SubgraphX identifies the malicious inheritance behavior of *Firefox* executing a template to generate multiple malware clones. However, it over-

looks sensitive file accesses, a detail exclusively captured by PROVEXPLAINER. PROVEXPLAINER comprehensively traced the malware kill chain from payload deployment and clone creation to the final step of accessing sensitive files.

7. Discussion and Future Work

GNN Model Capacity. *If decision trees trained with interpretable features provide accuracy comparable to GNN models, why do we need resource intensive GNN-based IDS?* In an IDS context, the automatic adaptability and generality provided by GNN models are necessary for quickly understanding the execution profiles of a wide variety of programs. DTs have many properties that, while unproblematic in an explanation setting, are highly undesirable for security detectors. Beyond the difference in expressive power, DTs require labelled data, which can be provided by the GNN in an explanation setting, but will not be available for security detection. Further, DTs rely on features that are derived from known data, so they are less able to generalize to unseen data. Therefore, for accurate and robust security detection, GNN models are strongly preferred. The DT’s expressive power is weaker in comparison to GNNs, and demands human understanding as a prerequisite for adequate feature engineering.

Is PROVEXPLAINER Model Agnostic? PROVEXPLAINER is model agnostic and works on black-box provenance-based IDS. This line of research is not novel, as previous works [67], have used decision trees as surrogate models for deep neural networks before. PROVEXPLAINER’s novelty stems from the development of interpretable graph features to enable surrogate DTs to provide explanations for decisions about heterogeneous graph data in the system provenance domain. The interpretation of advanced graph features in the system provenance domain enables domain experts to better understand the system-level evidence used by provenance-based IDS.

Capturing Subgraph Modifications. To address the weakness of whole-graph aggregation washing out the influence of small malicious subgraph modifications, PROVEXPLAINER’s DT explanations can be combined with general-purpose graph explanations techniques which were originally not suitable for the security domain, but can be tied to problem space actions by PROVEXPLAINER’s interpretable features. In future work, we will combine PROVEXPLAINER’s security-aware results that contain global perspective with the exploration stage of SubgraphX to better assist in identifying important subgraph structures.

Adversarial Manipulation of Graph Features. *What are the implications of attackers using knowledge of the graph structural features to design adversarial attacks against the explainer?* The explainer models used in PROVEXPLAINER is separate from the black-box detection model. Fooling both the interpretable surrogates and the underlying black-box model is the ideal case for an attacker seeking to avoid suspicion, and an attacker who can attack the explainer this way can also attack the detection model directly [46],

[75]. Creating robust detection and explanation systems that can withstand adversarial manipulation is a critical open research problem, and is beyond the scope of this work.

Reliable Explanation for Unreliable GNN Models. Recent studies have made significant strides in investigating evasive attack generation against provenance-based ML detectors [46], [75], a noteworthy perspective that raises questions about the robustness and stability of the ML models in question. However, the core underlying assumption driving model explainer research — that the stability and trustworthiness of ML models can always be assured — may not necessarily hold. In future work, we plan to investigate the efficacy of model explainers under adversarial conditions in ML models could enhance their reliability, providing insights into their performance in real-world adversarial scenarios and contribute to the development of robust systems.

Behavioral Query Language for System Provenance. In the future work we hope to develop a graph query language using defined behavioral features to support efficient retrieval of provenance records based on program behaviors. The graph query will be based on the graph features, allowing the operator to search for programs using high level descriptions of their behavior, which will be converted into graph features in the query engine. The direction will also benefit significantly from advancements in subgraph mining algorithms. Future works may consider specialized provenance storage systems to optimize data retrieval.

Support for Fine-Grained Detection Tasks. Recent developments in provenance-based security detection systems have trended towards fine-grained node and edge level anomaly detection [20], [57]. The explanation requirements of these detectors differ from those of whole-graph anomaly detectors and classifiers. In contrast to using explanations to narrow down the context for consideration by security practitioners, fine-grained models will need explainers to bring in relevant context to aid human analysis. Providing security-aware explanation support to advanced fine-grained security detectors is an exciting and important direction for future work.

8. Conclusion

We introduced PROVEXPLAINER that aims to bridge a critical gap in explainable ML for cybersecurity by providing transparent, human-interpretable insights into GNN-based decisions for provenance-based intrusion detection. By integrating security-aware subgraph patterns and structural graph features, PROVEXPLAINER enables effective instance-level explanations that are sensitive to both local and global graph properties. This dual-level interpretability is instrumental in addressing the opacity that limits the adoption of GNN-based models in critical security environments.

Through rigorous evaluation on real-world APT and Fileless Malware datasets, PROVEXPLAINER demonstrates superior fidelity and accuracy in its explanations, significantly outperforming existing SOTA GNN explainers across fidelity⁺, fidelity⁻, precision, and recall metrics. PROV-

EXPLAINER increases fidelity⁺ and decreases fidelity⁻ by 29% and 12%, and precision and recall by 27% and 25% over SOTA GNN explainers with respect to attack documentation prepared by security vendors and dataset authors. Importantly, while PROEXPLAINER structure-agnostic design allows for easy extension with additional security-aware features. This makes PROEXPLAINER not only an advancement in explainable AI for security applications but also a scalable and adaptable framework for future research and deployment in real-world security contexts.

References

- [1] A. Saini and H. Jazi, *North korea's lazarus apt leverages windows update client, github in latest campaign*, <https://tinyurl.com/mr4h7d35>, Accessed: April 6, 2023, 2022.
- [2] D. Legezo, *Wildpressure targets industrial in the middle east*, <https://tinyurl.com/mr2n8hdu>, Accessed: April 6, 2023, 2019.
- [3] D. E. Sanger and N. Perlroth, *U.s. said to find north korea ordered cyberattack on sony*, <https://tinyurl.com/5da2h9bx>, Accessed: April 6, 2023, 2014.
- [4] *Evasive attacker leverages solarwinds supply chain compromises with sunburst backdoor*, <https://tinyurl.com/bdz8s5yn>, Accessed: April 6, 2023, 2020.
- [5] G. E. Dahl, J. W. Stokes, L. Deng, and D. Yu, “Large-scale malware classification using random projections and neural networks,” in *2013 IEEE International Conference on Acoustics, Speech and Signal Processing*, IEEE, 2013.
- [6] D. Arp, M. Spreitzenbarth, M. Hubner, H. Gascon, K. Rieck, and C. Siemens, “Drebin: Effective and explainable detection of android malware in your pocket.,” in *Network and Distributed System Security Symposium (Ndss)*, Feb. 2014.
- [7] E. Gandotra, D. Bansal, and S. Sofat, “Malware analysis and classification: A survey,” *Journal of Information Security*, 2014.
- [8] J. Saxe and K. Berlin, “Deep neural network based malware detection using two dimensional binary program features,” in *2015 10th international conference on malicious and unwanted software (MALWARE)*, IEEE, 2015.
- [9] K. Grosse, N. Papernot, P. Manoharan, M. Backes, and P. McDaniel, “Adversarial perturbations against deep neural networks for malware classification,” *arXiv preprint arXiv:1606.04435*, 2016.
- [10] B. N. Narayanan, O. Djaneye-Boundjou, and T. M. Kebede, “Performance analysis of machine learning and pattern recognition algorithms for malware classification,” in *2016 IEEE National Aerospace and Electronics Conference (NAECON) and Ohio Innovation Summit (OIS)*, IEEE, 2016.
- [11] B. Kolosnjaji, A. Zarras, G. Webster, and C. Eckert, “Deep learning for classification of malware system call sequences,” in *Australasian Joint Conference on Artificial Intelligence*, 2016.
- [12] A. Javaid, Q. Niyaz, W. Sun, and M. Alam, “A deep learning approach for network intrusion detection system,” in *Proceedings of the 9th EAI International Conference on Bio-inspired Information and Communications Technologies (formerly BIONETICS)*, 2016.
- [13] T. A. Tang, L. Mhamdi, D. McLernon, S. A. R. Zaidi, and M. Ghogho, “Deep learning approach for network intrusion detection in software defined networking,” in *2016 IEEE International Conference on Wireless Networks and Mobile Communications (WINCOM)*, IEEE, 2016.
- [14] S. M. Milajerdi, R. Gjomemo, B. Eshete, R. Sekar, and V. N. Venkatakrishnan, “Holmes - real-time apt detection through correlation of suspicious information flows.,” in *IEEE Symposium on Security and Privacy (SP)*, 2019.
- [15] Q. Wang, W. U. Hassan, D. Li, *et al.*, “You are what you do: Hunting stealthy malware via data provenance analysis,” in *Network and Distributed System Security Symposium (NDSS)*, Feb. 2020.
- [16] X. Han, T. Pasquier, A. Bates, J. Mickens, and M. Seltzer, “Unicorn: Runtime provenance-based detector for advanced persistent threats,” in *Network and Distributed System Security Symposium (NDSS)*, Feb. 2020.
- [17] M. N. Hossain, S. Sheikhi, and R. Sekar, “Combating dependence explosion in forensic analysis using alternative tag propagation semantics,” in *IEEE Symposium on Security and Privacy (SP)*, 2020.
- [18] X. Han, X. Yu, T. Pasquier, *et al.*, “Sigl: Securing software installations through deep graph learning,” in *30th USENIX Security Symposium (SEC)*, 2021.
- [19] Z. Cheng, Q. Lv, J. Liang, *et al.*, “Kairos: Practical intrusion detection and investigation using whole-system provenance,” in *IEEE Symposium on Security and Privacy (SP)*, 2024.
- [20] M. U. Rehman, H. Ahmadi, and W. U. Hassan, “Flash: A comprehensive approach to intrusion detection via provenance graph representation learning,” in *IEEE Symposium on Security and Privacy (SP)*, 2024.
- [21] A. Goyal, G. Wang, and A. Bates, “R-caid: Embedding root cause analysis within provenance-based intrusion detection,” in *IEEE Symposium on Security and Privacy (SP)*, 2024.
- [22] *What is xdr?* <https://tinyurl.com/mrymbmd5>, Accessed: April 6, 2023, 2022.
- [23] P. Firstbrook and C. Lawson, *Gartner reprint*, <https://www.gartner.com/doc/reprints?id=1-27NCOQL7&ct=211014&st=sb>, Accessed: April 1, 2023, 2022.
- [24] Vendor, *Endpoint detection and response (edr) solutions reviews 2022 — gartner peer insights*, <http://tinyurl.com/spturarb>, Accessed: April 1, 2023, 2022.
- [25] P. A. Team, *What is endpoint detection and response (edr)? - palo alto networks*, <http://tinyurl.com/3kt8btd2>, Accessed: April 1, 2023, 2022.
- [26] G. Karantzas and C. Patsakis, “An empirical assessment of endpoint security systems against advanced persistent threats attack vectors,” *CoRR*, 2021.

[27] Z. Jia, Y. Xiong, Y. Nan, Y. Zhang, J. Zhao, and M. Wen, “[Magic]: Detecting advanced persistent threats via masked graph representation learning,” in *32nd USENIX Security Symposium (SEC)*, 2024.

[28] Z. Ying, D. Bourgeois, J. You, M. Zitnik, and J. Leskovec, “Gnnexplainer: Generating explanations for graph neural networks,” in *Neural Information Processing Systems (NeurIPS)*, 2019.

[29] D. Luo, W. Cheng, D. Xu, *et al.*, “Parameterized explainer for graph neural network,” 2020.

[30] H. Yuan, H. Yu, J. Wang, K. Li, and S. Ji, “On explainability of graph neural networks via subgraph explorations,” in *International Conference on Machine Learning (ICML)*, PMLR, 2021.

[31] A. Warnecke, D. Arp, C. Wressnegger, and K. Rieck, “Don’t paint it black: White-box explanations for deep learning in computer security,” *CoRR*, 2019.

[32] A. Warnecke, D. Arp, C. Wressnegger, and K. Rieck, “Evaluating explanation methods for deep learning in security,” in *2020 IEEE 7th European Symposium on Security and Privacy (EuroS&P)*, 2020.

[33] T. Ganz, P. Rall, M. Härterich, and K. Rieck, “Hunting for truth: Analyzing explanation methods in learning-based vulnerability discovery,” in *2023 IEEE 8th European Symposium on Security and Privacy (EuroS&P)*, 2023.

[34] DARPA, *Explainable artificial intelligence (xai)*, <http://tinyurl.com/3zxc37ac>, 2016.

[35] C. Rudin, “Stop explaining black box machine learning models for high stakes decisions and use interpretable models instead,” *Nature machine intelligence*, 2019.

[36] Z. C. Lipton, “The mythos of model interpretability: In machine learning, the concept of interpretability is both important and slippery.,” *ACM Queue*, 2018.

[37] C. Jiang, F. Coenen, and M. Zito, “A survey of frequent subgraph mining algorithms,” 2013.

[38] A. K. Sood and S. Zeadally, “Drive-by download attacks: A comparative study,” *IT Professional*, 2016.

[39] G. Phillips, *What is a drive-by download malware attack?* <http://tinyurl.com/yzbecv5>, 2021.

[40] *Trojan.win32.scar.ad*, <https://tinyurl.com/3sdj642z>, 2019.

[41] *Mimikatz*, <http://tinyurl.com/3styvesw>, (Accessed on 01/21/2024), 2018.

[42] G. O. Detecting and S. an APT41 Operation, *Mimikatz*, <http://tinyurl.com/mr4cdtyv>, (Accessed on 01/21/2024), 2023.

[43] F. Pierazzi, F. Pendlebury, J. Cortellazzi, and L. Cavallaro, “Intriguing properties of adversarial ml attacks in the problem space,” in *IEEE Symposium on Security and Privacy (SP)*, 2020.

[44] T. Ganz, M. Härterich, A. Warnecke, and K. Rieck, “Explaining graph neural networks for vulnerability discovery,” in *Proceedings of the 14th ACM Workshop on Artificial Intelligence and Security*, 2021.

[45] J. Griffith, D. Kong, A. Caro, *et al.*, “Scalable transparency architecture for research collaboration (starc)-darpa transparent computing (tc) program,” Raytheon BBN Technologies Corp. Cambridge United States, Tech. Rep.

[46] K. Mukherjee, J. Wiedemeier, T. Wang, *et al.*, “Evading provenance-based ml detectors with adversarial system actions,” in *32nd USENIX Security Symposium (SEC)*, 2023.

[47] F. Barr-Smith, X. Ugarte-Pedrero, M. Graziano, R. Spolaor, and I. Martinovic, “Survivalism: Systematic analysis of windows malware living-off-the-land,” in *IEEE Symposium on Security and Privacy (SP)*, 2021.

[48] S. T. King and P. M. Chen, “Backtracking intrusions,” in *USENIX Symposium on Operating Systems Design and Implementation (OSDI)*, 2003.

[49] M. A. Inam, Y. Chen, A. Goyal, *et al.*, “Sok: History is a vast early warning system: Auditing the provenance of system intrusions,” in *IEEE Symposium on Security and Privacy (SP)*, 2023.

[50] MITRE, *Mitre att&ck®*, <https://attack.mitre.org/>, Accessed: April 6, 2023.

[51] *Virustotal*, <https://www.virustotal.com/>, Accessed: April 6, 2023, 2021.

[52] *Metasploit*, <https://www.metasploit.com/>, (Accessed on 11/29/2021), 2021.

[53] *Cobalt strike — adversary simulation and red team operations*, <https://www.cobaltstrike.com/>, 2023.

[54] *Canvas*, <http://tinyurl.com/4bd7ann3>, 2023.

[55] S. Forrest, S. Hofmeyr, A. Somayaji, and T. Longstaff, “A sense of self for unix processes,” in *IEEE Symposium on Security and Privacy (SP)*, 1996.

[56] F. Yang, J. Xu, C. Xiong, Z. Li, and K. Zhang, “[Prographer]: An anomaly detection system based on provenance graph embedding,” in *32nd USENIX Security Symposium (SEC)*, 2023.

[57] J. Zengy, X. Wang, J. Liu, *et al.*, “Shadewatcher: Recommendation-guided cyber threat analysis using system audit records,” in *IEEE Symposium on Security and Privacy (SP)*, 2022.

[58] *Deep graph library: Easy deep learning on graphs*, <https://www.dgl.ai/>, (Accessed on 09/21/2021), 2022.

[59] K. Mukherjee and T. Wang, *Heterogeneous graph support for gnnexplainer*, <https://tinyurl.com/y25st3zp>, Accessed: November 6, 2023, 2022.

[60] K. Mukherjee and N. Baker, *Implemented pgexplainer for heterogeneous graph*, <https://tinyurl.com/jxxw32ws>, Accessed: November 6, 2023, 2023.

[61] K. Mukherjee, *Implemented pgexplainer for homogeneous graph*, <https://tinyurl.com/y66jhtr7>, Accessed: November 6, 2023, 2023.

[62] K. Mukherjee, *Implemented subgraphx explainer for homogeneous graph*, <https://tinyurl.com/yc6uf78a>, Accessed: November 6, 2023, 2023.

[63] K. Mukherjee, *Implemented subgraphx explainer for homogeneous graph*, <https://tinyurl.com/yc6uf78a>, Accessed: November 6, 2023, 2023.

[64] W. Guo, D. Mu, J. Xu, P. Su, G. Wang, and X. Xing, “Lemma: Explaining deep learning based security ap-

lications,” in *ACM conference on Computer and Communications Security (CCS)*, Nov. 2018.

[65] J. D. Herath, P. P. Wakodikar, P. Yang, and G. Yan, “Cfgexplainer: Explaining graph neural network-based malware classification from control flow graphs,” in *2022 52nd Annual IEEE/IFIP International Conference on Dependable Systems and Networks (DSN)*, 2022.

[66] M. Someya, Y. Otsubo, and A. Otsuka, “Fcgat: Interpretable malware classification method using function call graph and attention mechanism,” in *Network and Distributed System Security Symposium (NDSS)*, vol. 1, Feb. 2023.

[67] A. S. Jacobs, R. Beltaukov, W. Willinger, R. A. Ferreira, A. Gupta, and L. Z. Granville, “Ai/ml for network security: The emperor has no clothes,” in *ACM Conference on Computer and Communications Security (CCS)*, Nov. 2022.

[68] M. Kosan, S. Verma, B. Armagan, *et al.*, “Gnnx-bench: Unravelling the utility of perturbation-based gnn explainers through in-depth benchmarking,” 2023.

[69] *Canvas*, <http://tinyurl.com/y4wrf74u>, 2023.

[70] *Canvas*, <http://tinyurl.com/yaknev56>, 2023.

[71] *die.net, Linux man page*, <https://linux.die.net/man/>, 2017.

[72] H. Yuan, H. Yu, S. Gui, and S. Ji, “Explainability in graph neural networks: A taxonomic survey,” *arXiv preprint arXiv:2012.15445*, 2020.

[73] W. U. Hassan, S. Guo, D. Li, *et al.*, “Nodoze: Combating threat alert fatigue with automated provenance triage,” in *Network and Distributed System Security Symposium (NDSS)*, Feb. 2019.

[74] Y. Liu, M. Zhang, D. Li, *et al.*, “Towards a timely causality analysis for enterprise security,” in *Network and Distributed System Security Symposium (NDSS)*, Feb. 2018.

[75] A. Goyal, X. Han, G. Wang, and A. Bates, “Sometimes, you aren’t what you do: Mimicry attacks against provenance graph host intrusion detection systems,” in *Network and Distributed System Security Symposium (NDSS)*, Feb. 2023.

[76] M. J. Zaki, W. Meira Jr, and W. Meira, *Data Mining and Analysis: Fundamental Concepts and Algorithms*. Cambridge University Press, 2014.

[77] P. Veličković, G. Cucurull, A. Casanova, A. Romero, P. Lio, and Y. Bengio, “Graph attention networks,” *arXiv preprint arXiv:1710.10903*, 2017.

[78] W. Hamilton, Z. Ying, and J. Leskovec, “Inductive representation learning on large graphs,” 2017.

[79] A. Küchler, A. Mantovani, Y. Han, L. Bilge, and D. Balzarotti, “Does every second count? time-based evolution of malware behavior in sandboxes.,” in *Network and Distributed System Security Symposium (NDSS)*, Feb. 2021.

[80] E. Avllazagaj, Z. Zhu, L. Bilge, D. Balzarotti, and T. Dumitras, “When malware changed its mind: An empirical study of variable program behaviors in the real world,” in *30th USENIX Security Symposium (SEC)*, 2021.

[81] M. Team, *Event tracing*, <http://tinyurl.com/4usyncm>, 2021.

[82] Redhat, *The linux audit framework*, <https://github.com/linux-audit/>, 2017.

[83] scikit Team, *Scikit*, <https://scikit-learn.org/stable/>, 2021.

[84] K. P. Grammatikakis, I. Koufos, N. Kolokotronics, C. Vassilakis, and S. Shaeles, “Understanding and mitigating banking trojans: From zeus to emotet,” in *IEEE International Conference on Cyber Security and Resilience (CSR)*, 2021.

[85] M. ATT&CK®, *Exploitation for client execution*, <http://tinyurl.com/muhzctfb>, 2018.

[86] *Ntdll.dll*, <http://tinyurl.com/yc2z88px>, (Accessed on 01/21/2024), 2018.

[87] *Bcryptprimitives.dll*, <http://tinyurl.com/yvpesvzt>, (Accessed on 01/21/2024), 2018.

Appendix

1. Implementation

Our data collection module can operate on Windows systems by using the Windows ETW [81] and on Linux system by using Linux auditd [82] frameworks to collect relevant system calls regarding files, processes and network sockets. These include system calls for (1) file operations (e.g., `read()`, `write()`, `unlink()`), (3) network socket operations (e.g., `connect()`, `accept()`), (4) process operations (e.g., `create()`, `exec()`, and `exit()`). The system-level data is stored in a PostgreSQL database. Table 1 summarizes the event collection schema for our in-house deployment.

PROVEXPLAINER is implemented using python and graph generation framework is implemented in java. The GNN training and evaluation pipelines are implemented using Deep Graph Library (DGL) [58] framework, and the surrogate DTs are implemented using sklearn [83].

2. Dataset Statistics

Anomaly Detection Dataset. The dataset statistics for the anomaly detection dataset is seen in Table 4. The Fileless Malware samples were downloaded from [51] and selected from recent studies, [47], [79], [80], [84]. The benign provenance graphs for the anomaly detection dataset were sourced from the DARPA dataset, which contained 5,695 benign graphs with an average of 669.81 vertices and 982.18 edges (Table 4); the Fileless Malware dataset, which contained 19,422 benign graphs with an average of 60.44 vertices and 54.15 edges; and the APT dataset, which contained 6,291 benign graphs with an average of 55.94 vertices and 83.29 edges. The corresponding anomaly graphs are sourced from the same datasets: The DARPA dataset contained 30 anomalous graphs with an average of 777.08 vertices and

TABLE 4: APT and Fileless Malware graph statistics.

Applications	# of Benign Graphs	# of Anomaly Graphs	Avg # of Benign Nodes / Edges	Avg # of Anomaly Nodes / Edges
DARPA APT Dataset [45]				
Trace	1883	8	735.35 / 957.56	836.15 / 946.75
Theia	2858	9	559.47 / 979.59	913.91 / 987.31
FiveDirections	954	13	906.22 / 971.91	959.43 / 973.63
Average	1898.33	10.00	669.81 / 982.18	777.08 / 1011.19
APT Dataset from [46]				
Enterprise Supply-Chain	3079	1836	90.22 / 85.13	73.73 / 76.88
	3212	1092	65.02 / 40.77	61.09 / 54.33
Average	3145.50	1464.00	55.94 / 83.29	58.38 / 51.69
Fileless Malware from [47]				
wscript.exe	399	40	66.18 / 59.94	44.10 / 56.45
cscript.exe	876	11	88.56 / 81.58	87.36 / 101.54
reg.exe	309	116	60.18 / 52.93	78.91 / 131.87
python.exe	15585	426	89.95 / 83.15	57.98 / 79.33
explorer.exe	399	40	66.18 / 59.94	44.10 / 56.45
netsh.exe	621	7	44.08 / 37.49	38.42 / 52.28
net.exe	621	7	44.08 / 37.49	38.42 / 52.28
rundll32.exe	1632	443	52.42 / 46.42	51.97 / 81.31
mshta.exe	876	11	88.56 / 81.58	87.36 / 101.54
schtasks.exe	399	40	66.18 / 59.94	44.10 / 56.45
conhost.exe	309	116	60.18 / 52.93	78.91 / 131.87
svchost.exe	1632	443	52.42 / 46.42	51.97 / 81.31
Average	2667.00	90.84	60.44 / 54.15	63.72 / 89.93

1011.19 edges (Table 4); the Fileless Malware contained 1,043 anomalous graphs with an average of 63.72 vertices and 89.93 edges; and the APT dataset contained 2,928 graphs with an average of 58.38 vertices and 51.69 edges.

3. Ablation Study (using GraphSAGE)

The ablation study utilizing the GraphSAGE network revealed patterns consistent with those observed in the ablation study using GAT network §5.4. It was again noted that for Fileless Malware datasets the graph structural features provided better feature selection than subgraph patterns. This pattern is observed because the malware graphs are distinctively different when compared against their benign counter part. Finally, the pattern that subgraph patterns with the graph structures provided the best feature selection.

4. PROVEXPLAINER vs. SOTA Explainers

Similar to the GAT -based results, PROVEXPLAINER demonstrates superior performance across various datasets. The complexity of the provenance graphs, defined by their size and the nature of resource interactions, significantly influences the effectiveness of different explainers on specific datasets. For instance, on provenance graphs such as the APT graphs from [46], PGExplainer achieves the second-best performance. However, for the more complex or noisy DARPA APT graphs, GNNExplainer emerges as the second most effective method.

The structure of the Fileless Malware dataset’s malware graphs differs notably from APT attacks, particularly due to the characteristics of attack campaigns. In this context, SubgraphX outperforms both GNNExplainer and PGExplainer. SubgraphX specializes in isolating distinctive malicious subgraphs that, when removed, significantly alter model predic-

tions. Despite this strength, SubgraphX encounters limitations in scenarios where malware makes minimal, targeted changes to the system to evade detection, as observed in certain APT cases.

5. Case Studies: In-Depth Analysis

FiveDirections: Browser Extension. In the context of the described attack, where the drakon malware exploits the `firefox.exe` browser through a rogue extension (`pass_mgr`) the pattern #1 is created. Multiple instances of the malware process are created, each reading from the malicious files: `pass_mgr.exe` and `passwordfile.dat`. Additionally, they access essential dictionary files (`en-US.aff`) and cryptographic libraries (`bcryptprimitives.dll`) to maintain operational consistency, allowing them to conduct their malicious activities efficiently. The pattern #2 captures the data extraction behavior through sensitive file accesses. These malware access sensitive information and system configuration files like `WindowsShell.Manifest`, and `wintrust.dll`, along with initial malware files (`addons`, `tzres.dll`, `userenv.dll`).

GNNExplainer effectively identifies the malware template file present in `C:\ProgramFiles\MozillaFirefox\add-on\pass_mgr.exe` and the initial malware `pass_mgr.exe`. PGExplainer recognized the structures common across all attack graphs, particularly identifying file access of system libraries needed for malware operation `C:*\System32\driver`, `C:*\Windows\SysWOW64` and `C:*\AppData\Local\Temp`. SubgraphX performed at the same capacity as PGExplainer as it identified a different the structure of malware executing its payload from `C:*\Desktop*\add-on`, reading sensitive files from `C:*\ProgramFiles\MozillaFirefox*`, and extracting them through `C:*\admin\AppData*`. This is partly due to its foundation on Monte Carlo Tree Search (MCTS), incorporating nondeterministic exploitation and exploration stages. In the absence of attribute information in the GNN, the exploitation stage lacks guidance. But, when SubgraphX correctly identifies a substructure for exploitation, the exploration of MCTS proves effective.

FiveDirections: Copykatz. The pattern #2 starts its kill chain stage of initial access [85] by writing and executes a malware masquerading as `firefox.exe` which contains the Mimikatz and Copykatz modules. `ntdll.dll` [86] includes multiple kernel-mode functions which enables the “Windows Application Programming Interface (API)” and `bcryptprimitives.dll` [87] contain functions implementing cryptographic primitives, which are essential for Mimikatz [41] and Copykatz.

The `firefox.exe` malware write its payload into temporary files, such as `virtuous` and `tropical`. These files are then executed by malware in the system creating pattern #5. Subsequently, another malicious instance of the `firefox.exe` malware initiates a chain or read-execute

TABLE 5: Agreement of surrogate DTs with the GraphSAGE model across different feature subsets. The best feature subsets are highlighted.

Dataset	Top- K Subgraphs					All Top 5 Subgraphs	Graph Structural Features					All Graph Structural Feat.	All Features	
	1	2	3	4	5		Deg. Cen.	Clos. Cen.	Bet. Cen	Eig. Cen.	Clus. Coeff.	Clus. Tri.		
APT Dataset from [46]														
Enterprise Supply-Chain	0.91 (-0.03)	0.91 (-0.03)	0.91 (-0.03)	0.91 (-0.03)	0.91 (-0.03)	0.91 (-0.03)	0.91 (-0.03)	0.92 (-0.02)	0.92 (-0.02)	0.92 (-0.02)	0.92 (-0.02)	0.94 (+0.00)	0.94 (+0.00)	0.94
	0.77 (-0.20)	0.88 (-0.09)	0.89 (-0.08)	0.90 (-0.06)	0.90 (-0.06)	0.90 (-0.06)	0.90 (-0.06)	0.96 (-0.00)	0.96 (-0.00)	0.96 (-0.00)	0.97 (+0.00)	0.97 (+0.00)	0.97 (+0.00)	0.97
Average	0.84 (-0.12)	0.90 (-0.06)	0.90 (-0.06)	0.91 (-0.04)	0.91 (-0.04)	0.91 (-0.04)	0.91 (-0.04)	0.94 (-0.01)	0.94 (-0.01)	0.94 (-0.01)	0.95 (-0.01)	0.95 (+0.00)	0.95 (+0.00)	0.95
DARPA APT Dataset [45]														
FiveDirections	0.82 (+0.02)	0.80 (+0.00)	0.82 (+0.02)	0.82 (+0.02)	0.82 (+0.02)	0.82 (+0.02)	0.82 (+0.02)	0.82 (+0.02)	0.82 (+0.02)	0.82 (+0.02)	0.80 (+0.00)	0.82 (+0.02)	0.80 (+0.00)	0.80
Trace	0.87 (+0.00)	0.87 (+0.00)	0.87 (+0.00)	0.87 (+0.00)	0.93 (+0.07)	0.87 (+0.00)	0.93 (+0.07)	0.87 (+0.00)	0.87 (+0.00)	0.87 (+0.00)	0.93 (+0.07)	0.87 (+0.00)	0.87 (+0.00)	0.87
Theia	0.78 (-0.17)	0.78 (-0.17)	0.83 (-0.11)	0.83 (-0.11)	0.83 (-0.11)	0.83 (-0.11)	0.83 (-0.11)	0.83 (-0.11)	0.83 (-0.11)	0.83 (-0.11)	0.94 (+0.00)	0.94 (+0.00)	0.94 (+0.00)	0.94
Average	0.82 (-0.05)	0.82 (-0.06)	0.84 (-0.03)	0.84 (-0.03)	0.86 (-0.01)	0.84 (-0.03)	0.86 (-0.01)	0.86 (-0.01)	0.86 (-0.01)	0.86 (-0.01)	0.90 (+0.03)	0.90 (+0.03)	0.88 (+0.01)	0.89
Fileless Malware from [47]														
conhost	0.84 (-0.09)	0.89 (-0.04)	0.89 (-0.04)	0.89 (-0.04)	0.89 (-0.04)	0.89 (-0.04)	0.89 (-0.04)	0.89 (-0.04)	0.89 (-0.04)	0.89 (-0.04)	0.93 (+0.00)	0.93 (+0.00)	0.93 (+0.00)	0.93
explorer	0.72 (-0.26)	0.89 (-0.09)	0.91 (-0.07)	0.91 (-0.07)	0.89 (-0.09)	0.91 (-0.07)	0.89 (-0.09)	0.91 (-0.07)	0.91 (-0.07)	0.91 (-0.07)	0.98 (+0.00)	1.00 (+0.02)	1.00 (+0.02)	1.00
net	0.94 (-0.02)	0.94 (-0.02)	0.94 (-0.02)	0.94 (-0.02)	0.94 (-0.02)	0.94 (-0.02)	0.94 (-0.02)	0.94 (-0.02)	0.94 (-0.02)	0.94 (-0.02)	0.97 (+0.00)	0.97 (+0.00)	0.97 (+0.00)	0.97
reg	0.92 (-0.08)	0.92 (-0.08)	0.92 (-0.08)	0.92 (-0.08)	0.92 (-0.08)	0.92 (-0.08)	0.92 (-0.08)	0.92 (-0.08)	0.92 (-0.08)	0.92 (-0.08)	1.00 (+0.00)	1.00 (+0.00)	1.00 (+0.00)	1.00
wscript	0.89 (-0.07)	0.89 (-0.07)	0.89 (-0.07)	0.89 (-0.07)	0.89 (-0.07)	0.89 (-0.07)	0.89 (-0.07)	0.89 (-0.07)	0.89 (-0.07)	0.89 (-0.07)	0.95 (+0.00)	0.95 (+0.00)	0.95 (+0.00)	0.95
cscript	0.86 (-0.14)	0.86 (-0.14)	0.93 (-0.07)	0.93 (-0.07)	1.00 (+0.00)	0.93 (-0.07)	1.00 (+0.00)	1.00 (+0.00)	1.00 (+0.00)	1.00 (+0.00)	1.00 (+0.00)	1.00 (+0.00)	1.00 (+0.00)	1.00
mshta	0.85 (+0.00)	0.85 (+0.00)	0.85 (+0.00)	0.85 (+0.00)	0.85 (+0.00)	0.85 (+0.00)	0.85 (+0.00)	0.85 (+0.00)	0.85 (+0.00)	0.85 (+0.00)	1.00 (+0.15)	0.85 (+0.00)	0.85 (+0.00)	0.85
netsh	0.93 (-0.04)	0.91 (-0.07)	0.89 (-0.09)	0.89 (-0.09)	0.89 (-0.09)	0.89 (-0.09)	0.89 (-0.09)	0.89 (-0.09)	0.89 (-0.09)	0.89 (-0.09)	0.98 (+0.00)	0.98 (+0.00)	0.98 (+0.00)	0.98
python	0.58 (-0.41)	0.65 (-0.34)	0.65 (-0.34)	0.66 (-0.33)	0.64 (-0.35)	0.66 (-0.33)	0.64 (-0.35)	0.64 (-0.35)	0.64 (-0.35)	0.64 (-0.35)	0.93 (-0.06)	0.93 (-0.06)	0.93 (-0.06)	0.93
rundll32	0.85 (-0.10)	0.85 (-0.10)	0.85 (-0.10)	0.85 (-0.10)	0.85 (-0.10)	0.85 (-0.10)	0.85 (-0.10)	0.85 (-0.10)	0.85 (-0.10)	0.85 (-0.10)	0.96 (+0.00)	0.96 (+0.00)	0.96 (+0.00)	0.96
schtasks	0.98 (-0.02)	0.98 (-0.02)	0.98 (-0.02)	0.98 (-0.02)	0.98 (-0.02)	0.98 (-0.02)	0.98 (-0.02)	0.98 (-0.02)	0.98 (-0.02)	0.98 (-0.02)	1.00 (+0.00)	1.00 (+0.00)	1.00 (+0.00)	1.00
Average	0.86 (-0.10)	0.88 (-0.08)	0.89 (-0.08)	0.90 (-0.07)	0.90 (-0.07)	0.90 (-0.07)	0.90 (-0.07)	0.94 (-0.03)	0.94 (-0.03)	0.94 (-0.03)	0.97 (+0.00)	0.97 (+0.00)	0.97 (+0.00)	0.97

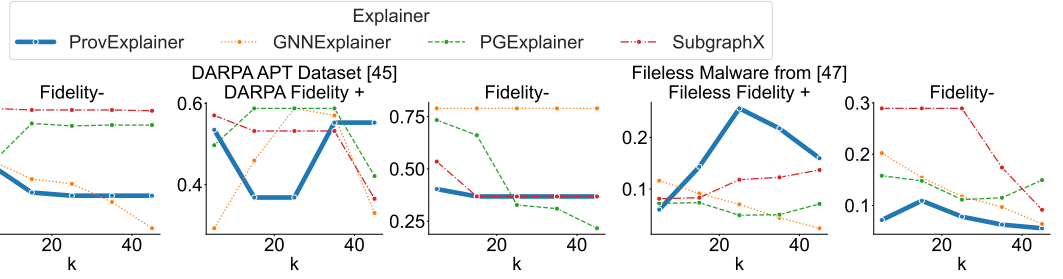


Figure 7: Effectiveness of GraphSAGE explainers in identifying prediction-relevant graph structures using fidelity⁺ and fidelity⁻.

cycle by executing the malware template as well as making external IP connections. This dependency correlation between the malware and its parent is characterized by inheritance, where the children require the same system library files as the parent to function correctly. The DLLs involved are read from `ProgramFiles` and `System32`.

GNNEExplainer and PGExplainer correctly identified the data extraction stage where four malicious `firefox.exe` processes make C2 connections to the external IPs (202.179.137.58 and 217.160.205.44). `firefox.exe` was invoked by malware masquerading as `runtimebroker.exe`, so if GNNEExplainer masks out the process creation edge of the children `firefox.exe`, that would lead to a graph cut with two separate graphs, leading to a change in the prediction. SubgraphX also highlighted similar `firefox.exe` processes that are created by the first `runtimebroker.exe`, but instead of making external C2 connection it created another `firefox.exe` process for rendering content from localhost (127.0.0.1).

Trace: Phishing E-mail. The pattern #2 captured the staging behavior of the Trojan. The Trojan was downloaded from www.nasa.ng, executed and replicated itself within the system. Specifically, the malware named `nasa.ng` is placed in `/home/admin/.mozilla/firefox/` and `/usr/local/firefox-54.0.1/obj-x86_64-pc-linux-gnu/`. The Trojan created new malware with benign names such as `firefox` to

effectively evade detectors, to replicate unhindered and overloaded the system with malicious processes. After the malware successfully staged, the malware masquerading as `/bin/sh` to read the malicious script staged in `(/etc/update-motd.d/00-header/)` and executed it to create multiple copies of itself. The malware reads various system configuration files present in `/etc/protocols/`, `/etc/lsb-release/`, and `/etc/hosts.deny/`. Reading sensitive system configuration files are essential to build the system profile. The pattern #5 captured the dependency correlation of the malware created that inherited configurations.

Ultimately, the malware completes its target of reading sensitive system files from `/etc/fonts/conf.d/`, `/usr/lib/x86_64-linux-gnu/`, and `/usr/share/X11/local/`. These activities are aimed at gathering system information to create a profile of the company and the devices in use. The attacker wants to create a profile of the victim environment to ensure their malware can effectively leverage system libraries to complete their objective. There is an overlap in the files (present in `\etc\hosts` and `/usr/lib/x86_64-linux-gnu/*`) involved in the pattern #2 and pattern #5 operations because the malware replicates itself probing and inheriting the functional dependencies of its parent.

GNNEExplainer was able to correctly capture the staging behavior where the malware from `nasa.ng` read shared li-

brary (/usr/lib/x86_64-linux-gnu/*.so.*) and cache file (/usr/share/applications/mimeinfo.cache, /usr/lib/x86_64-linux-gnu/*/ loaders.cache). PGExplainer incorrectly indicated benign substructures, but SubgraphX correctly captured the inheritance behavior of firefox.exe executing multiple times with the argument file <http://www.nasa.ng/>, to create the malware clones from the template. SOTA explainers missed the malware’s ultimate goal of reading sensitive files, which was only captured by PROVEXPLAINER.